Journal of Sol-Gel Science and Technology

Poly (m-phenylene isophthalamide)/Graphene Composite Aerogels with Enhanced Compressive Shape Stability for Thermal Insulation

--Manuscript Draft--

Manuscript Number:	JSST-D-20-00329R1
Full Title:	Poly (m-phenylene isophthalamide)/Graphene Composite Aerogels with Enhanced Compressive Shape Stability for Thermal Insulation
Article Type:	Original Paper
Keywords:	Graphene; Poly (m-phenylene isophthalamide); Composite Aerogels; Compressive Shape Stability; Thermal Insulation
Corresponding Author:	Xiaomeng Zhou, Ph.D. Civil Aviation University of China Tianjin, Tianjin CHINA
Corresponding Author Secondary Information:	
Corresponding Author's Institution:	Civil Aviation University of China
Corresponding Author's Secondary Institution:	
First Author:	Weiwang Chen, Ph.D.
First Author Secondary Information:	
Order of Authors:	Weiwang Chen, Ph.D.
	Sha Liu
	Yutong Dong
	Xiaomeng Zhou, Ph.D.
	Fenglei Zhou
Order of Authors Secondary Information:	
Funding Information:	National Natural Science Foundation of China (51904312) — Dr. Weiwang Chen
Abstract:	To develop graphene-based composite aerogels with improved compressive shape stability that suitable for high temperature applications, poly (m-phenylene isophthalamide, PMIA) with excellent heat resistance and flame retardancy was used as the supporting material. The effects of PMIA content on aerogel morphology, structure, mechanical and thermal properties were discussed. Unlike other polymers, PMIA in the composite aerogels appeared as separate or stacked particles instead of interconnected framework or uniform coatings. Higher PMIA content tended to result in denser aerogels with smaller pores and thinner graphene sheet walls. The densified structure with plenty of PMIA particles incorporated was found to make the aerogel more rigid and less flexible. Their compressive strength therefore was greatly enhanced. Besides, it was also observed that the thermal conductivity of the prepared aerogels increased with the increase of PMIA content. Nevertheless, their thermal conductivity was still less than 0.045 W·m-1·K-1, indicative of considerable thermal insulation ability. Given that, the prepared composite aerogels with enhanced compressive shape stability may have a broad application prospect in thermal insulation.
Response to Reviewers:	
Section/Category:	Nano- and macroporous materials (aerogels, xerogels, cryogels, etc.)
Additional Information:	
Question	**Response**

Poly (*m*-phenylene isophthalamide)/Graphene Composite Aerogels with Enhanced Compressive Shape Stability for Thermal Insulation

Weiwang Chen, [1] Sha Liu, [1] Yutong Dong, [1] Xiaomeng Zhou, [1*] Fenglei Zhou, [2, 3]

[1] *Key Laboratory of Civil Aviation Thermal Hazards Prevention and Emergency Response, Civil Aviation University of China, Tianjin, 300300, P. R. China*

[2] *Centre for Medical Image Computing, Department of Computer Science, University College London, London, WC1V 6LJ, UK*
[3] *College of Textiles and Clothing, Qingdao University, Qingdao, 266071, P. R. China*

Corresponding author: X. Zhou (E-mail: zhouxm@nankai.edu.cn)

ABSTRACT

To develop graphene-based composite aerogels with improved compressive shape stability that suitable for high temperature applications, poly (*m*-phenylene isophthalamide, PMIA) with excellent heat resistance and flame retardancy was used as the supporting material. The effects of PMIA content on aerogel morphology, structure, mechanical and thermal properties were discussed. Unlike other polymers, PMIA in the composite aerogels appeared as separate or stacked particles instead of interconnected framework or uniform coatings. Higher PMIA content tended to result in denser aerogels with smaller pores and thinner graphene sheet walls. The densified structure with plenty of PMIA particles incorporated was found to make the aerogel more rigid and less flexible. Their compressive strength therefore was greatly enhanced. Besides, it was also observed that the thermal conductivity of the prepared aerogels increased with the increase of PMIA content. Nevertheless, their thermal conductivity was still less than 0.045 W·m^{-1}·K^{-1}, indicative of considerable thermal insulation ability. Given that, the prepared composite aerogels with enhanced compressive shape stability may have a broad application prospect in thermal insulation.

KEYWORDS

Graphene; Poly (*m*-phenylene isophthalamide); Composite Aerogels; Compressive Shape Stability; Thermal Insulation.

Introduction

Due to their ultralight density, large pore volume and tunable porosity, aerogels are of great interest for many applications in the fields of thermal regulation, waste disposal, catalysis, electrochemistry, etc.[1-5] There are a wide range of aerogels available, such as SiO_2 aerogels, Al_2O_3 aerogels, carbon aerogels, and so on [6-9]. Among them, graphene aerogels (GAs, also known as graphene sponges) are very attractive in recent years [10]. Their unique micro-nano porous structure contributes themselves remarkable thermal insulation ability, by depressing gaseous and solid heat transfer. Besides, the graphene's perfect opacity bring GAs good extinction coefficient, which can block thermal radiation and therefore reduce heat transfer further [11]. Unfortunately, these graphene aerogels are always fragile, and easy to collapse or deform during the process of handling [12-14].

Over the last few years, considerable efforts have been made to enhance the mechanical strength of the delicate GAs [15-22]. An effective approach is to introduce chemical crosslinking agents into GA system, forming strong interactions among graphene sheets. For example, Huang et al. (2013) chose polyethylenimine (PEI) with high primary amine density for crosslinking and obtained composite aerogels with Young's modulus up to 20 MPa [15]. Besides, strength enhancement can also be achieved by physical filling or blending modifications. By incorporating fibrous or polymeric supporting additives into the aerogel, mechanical property of the fragile GAs can be improved. These physically modified aerogels can be roughly divided into two groups: the premixed composite aerogels and the post-impregnated ones, depending on the addition time of supporting additives. Yue et al. (2017) reported a series of composite aerogels reinforced by ultrafine quartz fibers [16]. The fibers were added before gelation and brought the aerogels good tensile strength by weakening their brittleness. Ha et al. (2015) also described a similar strategy to overcome the brittle limitation of GAs [17]. In their study, a certain amount of poly (acrylic acid) solution was added prior to gelation as well, expressed as one-step synthesis of composite aerogel. Some other polymers, such as poly (ethylene oxide) (PEO) [18], poly (amic acid) (PAA, the precursor of polyimide) [20,19] etc., were also used as premixed supporting materials for GAs. As to the post-impregnated ones, they are usually prepared by backfilling polymers into the pores of the as-prepared GAs. Ye et al. (2014), for example, pressed GAs into cyclohexane solution with different poly (styrene-b-(ethylene-co-butylene)-b-styrene) (SEBS) contents, resulting in polymer-infiltrated composites with porous structure [21]. Hu et al. (2014) immersed their as-prepared compressible aerogels into a hexane solution of poly (dimethyl siloxane, PDMS) monomer [22]. The aerogel's outer surface as well as their inner pore walls therefore were coated with an integrated uniform polymer layer, resulting in composite aerogels with enhanced compressive strength. The post-impregnated strategy, however, is usually time consuming and difficult to control compared to the pre-mixing method. In addition, most of the supporting polymers used so far are thermoplastic, water-soluble or flammable, and cannot survive in fire scenarios that are full of fire-fighting water and high temperature flames. More appropriate polymers with better heat and flame resistance thus need to be considered as potential replacements.

In the present study, poly (*m*-phenylene isophthalamide) (PMIA) with excellent heat resistant and flame retardant properties [23] was employed as the supporting material for developing a new type of graphene-based composite aerogel. The composites (i.e. PGAs) were prepared by premixing a certain amount of PMIA solution in GO suspension before the classical self-assembly reduction and freeze-drying procedure. The morphology, thermal and mechanical properties of the obtained aerogels were then characterized. Experimental results reveal that the added PMIA presents as numerous particles, which innovates the existence of supporting polymers. These PMIA particles can not only reduce the size of aerogel pores but also provide "stepping stones" for graphene stacking. The densified structure brought PGAs with enhanced compressive strength, which can support more than 2000 times its own weight. Besides, these composite aerogels were found to suffer gradual degradation in thermal conductivity with increasing PMIA content, but were still good at thermal insulation and heat resistance. There is reason to believe that the resultant composite aerogels with enhance compressive shape stability will have broad prospect in the field of high-temperature thermal protection.

Materials and methods

Materials

GO dispersion (4 mg·mL^{-1}) in N, N-Dimethylformamide (DMF) was purchased from Carmery Materials Technology Co., Ltd (Taiyuan, China). Commercial PMIA short fibers (Mw≈200,000 g·mol^{-1}) were supplied by Tayho Advanced Materials Co., Ltd (Yantai, China). Other reagents, i.e. N, N-Dimethylacetamide (DMAc), lithium chloride (LiCl), *m*-Phenylenediamine (MPD), were all obtained from Sinopharm Chemical Reagent Co., Ltd (Beijing, China) and were used as received without further purification. Of the three, MPD acted as the reducing and cross-linking agent, to introduce N atoms into graphene sheets and at the same time assemble these sheets together to form wet gels. DMAC and LiCl were used together to provide a solvent system that can dissolve PMIA short fibers.

Preparation of pristine solutions

PMIA pristine solution was prepared by completely dissolving a certain amount of PMIA short fibers in LiCl/DMAc solvent system, as according to the reported procedure in our previous work [24]. Another pristine solution, MPD/LiCl/DMAc solution, was also prepared in a similar way. The mass fractions of PMIA and LiCl in PMIA pristine solution were controlled to be 10 % and 2 %, respectively. For the MPD pristine solution, the mass fraction values of MPD and LiCl were set as 10% and 5%, respectively.

Preparation of PGA composite aerogels

A series of PMIA-reinforced graphene aerogels were prepared according to the classical freeze-drying process, but in a non-aqueous solution system (see the schematic diagram in Fig. 1). In a typical procedure, 1g of MPD pristine solution was firstly transferred to each glass vial (20 mL). Then, varying amounts of GO suspension (($6-X$) g, $X = 0, 0.5, 1, 1.5, 2$, or 3g) were added, followed by a brief ultrasonic treatment. The well-sealed vials with uniform suspensions inside were scheduled to undergo a 3h static pre-reduction process at 60 ^{o}C, to reduce GO sheets partially. After that, the pre-reduced dispersions were mixed with X g of PMIA pristine solution, and were vigorously shook and ultrasonically dispersed before a two-step thermal gelatinization (80 ^{o}C for 24 h and 110 ^{o}C for another 6 h). During the gelation process, MPD molecules were grafted onto graphene sheets or doped inside, through the reactions of $–NH_2$ with the oxygen functional groups of GO sheets. As a result, black wet gels were formed. Before carrying out the freeze-drying process, the as-formed wet gels were dialyzed for several times by using an ethanol solution (10 vol. %). This step mainly meant to remove residual impurities and to adjust the temperature of icing. To further remove organic groups that easy to decompose, the freeze-dried composite aerogels were then thermally annealed at 230 °C for 6 h. The composite aerogels with *X* g PMIA added thus can be finally obtained, recorded as PGA-*X* in the following parts.

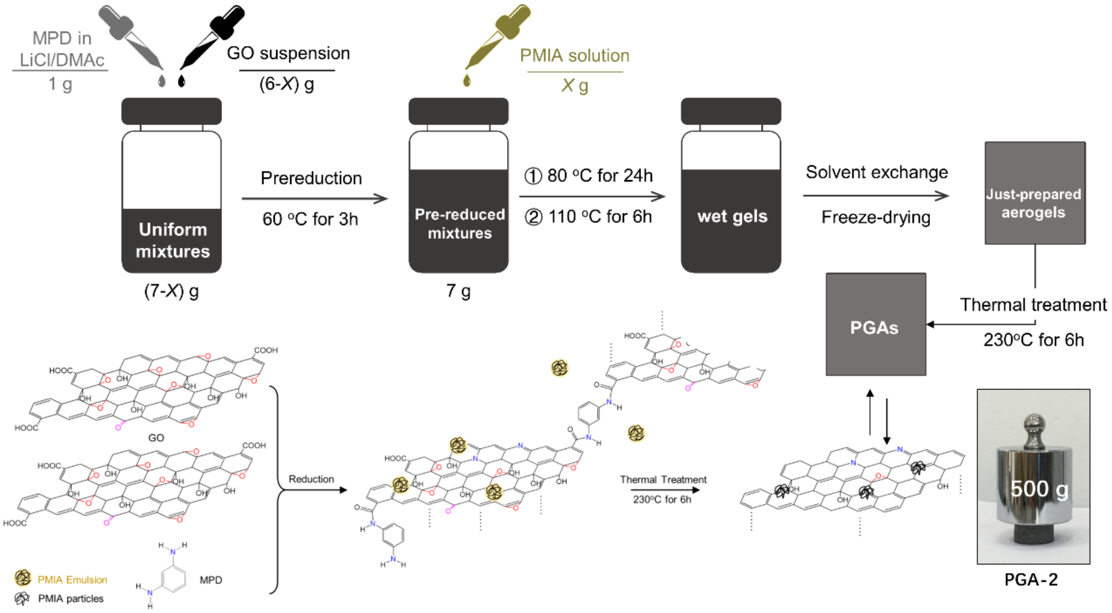

Figure 1 Typical procedure for the preparation of PGAs.

Characterization

The bulk density of the prepared composite aerogels (i.e. PGAs) was calculated from the mass-to-volume ratios. The microstructure of PGAs was observed by field emission scanning electron microscopy (FE-SEM, 1530VP, LEO, Germany). Before SEM observation, all specimens were coated with a sputter coater (SC7620, Quorum/Polaron, UK) to render them better electrical conductivity. Besides, their chemical structure and surface composition were characterized by X-ray photoelectron spectroscopy (XPS, TESCALAB 250Xi, Thermo Scientific, USA) and Fourier transform infrared spectroscopy (FTIR, Nexus870, Nicolet, USA). The FTIR data were recorded over the range of 600~4000 cm^{-1} with a wavenumber resolution of 2 cm^{-1}. Nitrogen adsorption-desorption tests were also performed, in a Brunauer-Emmett-Teller analyzer (BET, ASAP 2640, Micromeritics, USA). Specific surface area and pore size distribution used for analysis were obtained from the BET and Barrett-Joyner-Halenda (BJH) methods, respectively. In addition, thermal decomposition properties of the prepared aerogels were also measured by using a thermo-gravimetric analyzer (TGA, TGA/SDTA851^e, Mettler-Toledo, Switzerland). The aerogel samples were heated from room temperature (RT) to 700 ^{o}C at a heating rate of 20 ^{o}C·min^{-1} in nitrogen or air atmosphere. Thermal conductive values were obtained by a TPS2500 apparatus (Hot Disk, Sweden). Mechanical analysis was carried out by an electronic universal material testing machine (AGS-X, Shimadzu, Japan). The crosshead speed and pre-tension values during compression were set as 2 mm·min^{-1} and 0.05 N, respectively.

Results and discussion

Microstructure and chemical composition characterization

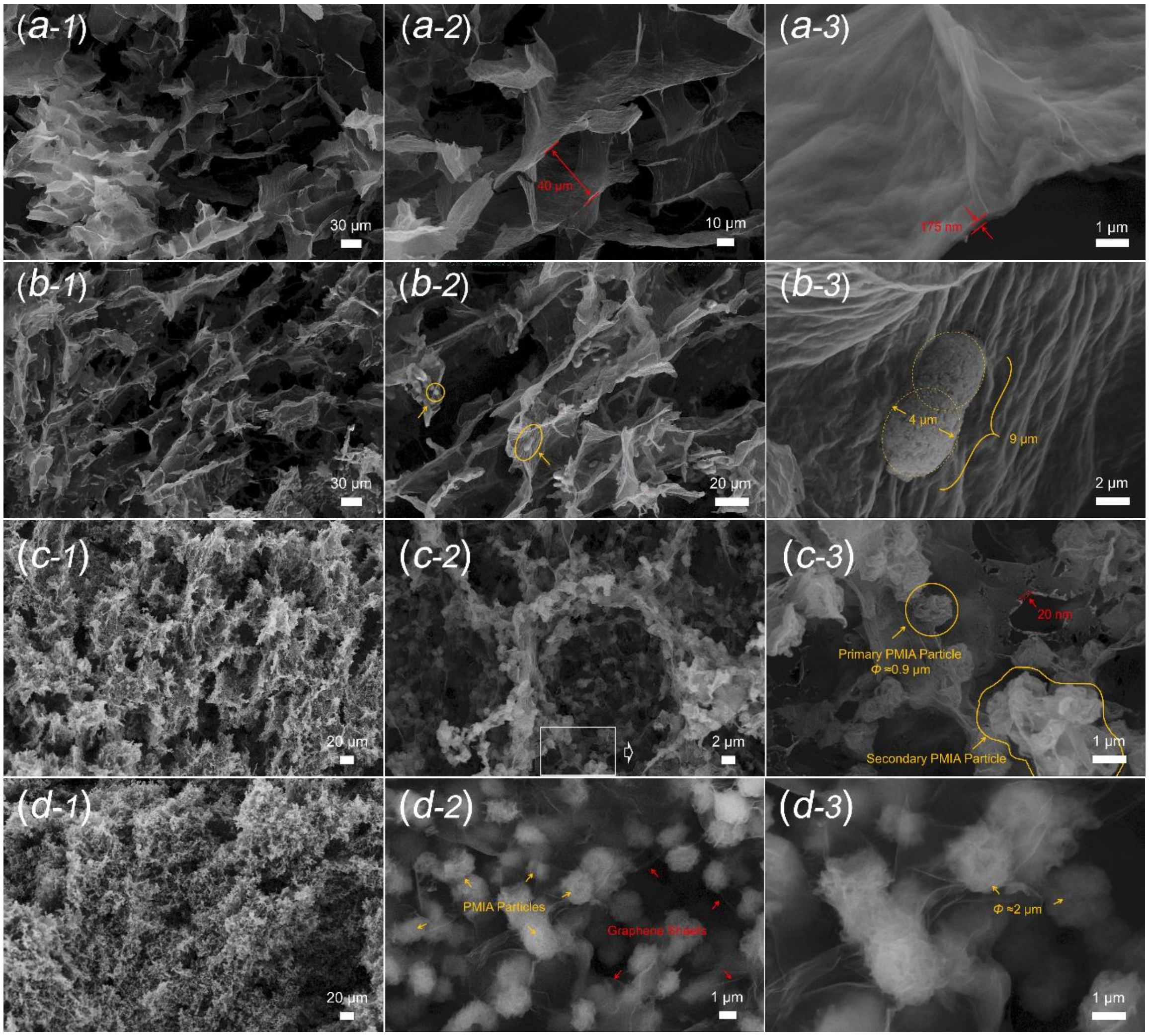

Figure 2 Microstructure of PGAs with different PMIA incorporated: **a** PGA-0, **b** PGA-1, **c** PGA-2, and **d** PGA-3.

Fig. 2a-d displays the cross-sectional morphology of the prepared composite aerogels. It is obvious that the pristine aerogel without PMIA incorporated, i.e. PGA-0 in Fig. 2a, has a typical honeycomb microporous structure with aerogel pore size ranging from tens to hundreds of micrometers. The effect of crystal squeezing during freezing should be responsible for the formation of these pores [25,26]. Before this, a wet gel must be formed. To achieve this, the reducing agent MPD is indispensable. It can react with oxygen functional groups of GO sheets, and drive these sheets to self-assemble under the effects of π-π interaction, hydrogen bonding and covalent connection [10,27,28]. The shale-like pore wall marked in Fig. 2a-3 was measured to be 175 nm thick, about 500 times the thickness of monolayer graphene sheet. Once a certain amount of PMIA solution (0.5 g) was added, a large number of irregular PMIA particles appeared on the surface of GO sheets (see Fig. 2b). There should be two reasons. The first is the existence of phase separation. According to Yao et al. (2010)[29], the solubility of PMIA in DMF is poor, even in the presence of LiCl. Their experimental results indicated that PMIA can only swells in LiCl/DMF solvent system with a LiCl fraction of 2wt.%. However, under the same LiCl content, PMIA can easily be dissolved into LiCl/DMAc solvent system to form a homogeneous solution. In this case, adding PMIA solution in GO/DMF suspension will inevitably cause phase separation. That is, with the help of ultrasonic treatment, PMIA pristine solution added exists as emulsion particles in GO/DMF solution system, forming a PMIA rich phase and another graphene rich phase. Besides, due to the mutual solubility of DMF and DMAc, a certain amount of DMAc in PMIA emulsion particles therefore tends to be extracted, resulting in interface or even particle precipitation. These uniformly dispersed particles then adhere to graphene sheets under the action of intermolecular forces, and are embedded within the wet gel along with thermal gelatinization. The possible procedure for the formation of PMIA particles was given in Fig.3. The second reason should be the uneven distribution of PMIA on GO sheets with very large surface areas. BET result showed that the specific surface area of the prepared pristine aerogel without PMIA incorporated was 235.4 $m^2 \cdot g^{-1}$. The effective attachment area of graphene sheets in PGA-0.5 thus was calculated to be several square meters. The distribution of PMIA in

PGA-0.5 therefore can be equated to an almost uniform dispersion of 0.05g PMIA on a single piece of several square meter large graphene substrate. Given its huge molecular weight (~200,000 g·mol^{-1}) and sufficient intermolecular entanglements, PMIA itself cannot cover the "graphene substrate" evenly in a thin film but appears as scattered droplets. Such droplets then precipitate as separate or stacked PMIA particles in Fig. 2.

As the content of PMIA increased, aerogel pores that can be seen everywhere tended to be filled. The possible mechanism responsible for this change can be explained from two aspects. Firstly, a higher PMIA content leads to more PMIA particles per unit volume, which can act as barriers to prevent GO sheets from stacking. The number of pores per unit volume therefore increases dramatically. That is, the aerogel pores formed during gelatinization are smaller under higher PMIA contents and are easier to be filled. Secondly, a higher PMIA content also means that more PMIA particles are available to act as fillers. These could explain why PGA-2 had more compact pores with more PMIA particles filled (see Fig. 2c), so as the PGA-3 in Fig. 2d. Interestingly, the microstructure of PGA-3 was found to be similar to that of SiO_2 aerogels [30]. Their difference in structure mainly lied in the size of primary particles and whether or not laminated graphene sheets were present. For pure SiO_2 aerogels, their primary particles are about tens of nanometers in diameter, much smaller than that of PMIA particles in the present study (~2 μm in Fig. 2d-3). In addition, the pore walls in PGA-3 seemed to be much thinner and lighter than other PGAs, just like "silk scarfs" with PMIA particles wrapped inside.

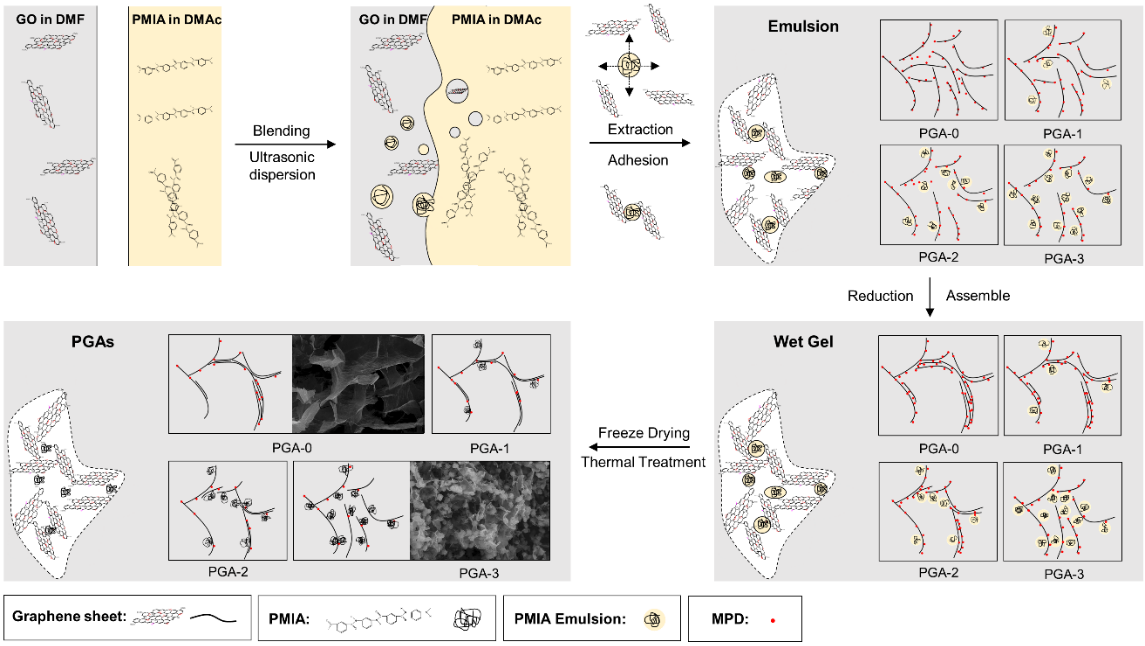

Figure 3 The possible mechanism for the formation of PMIA particles.

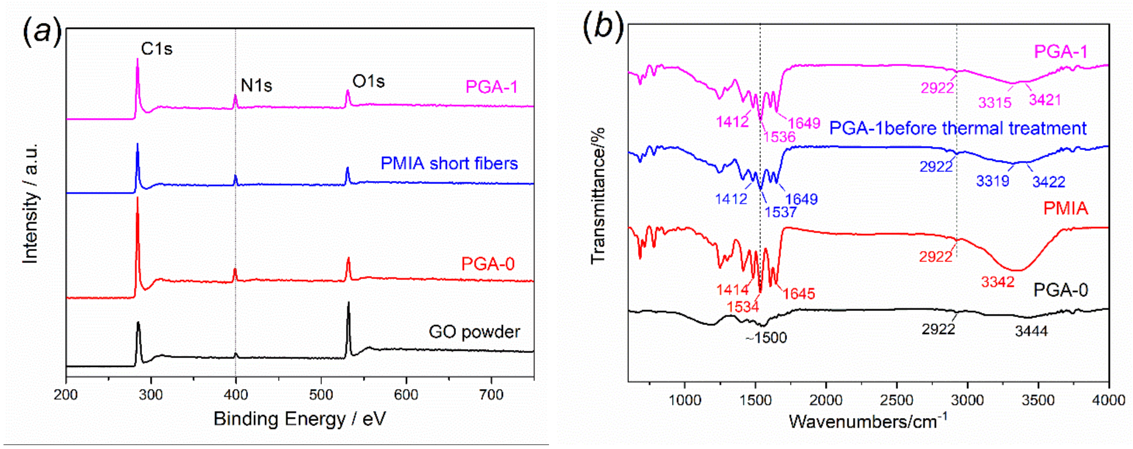

Figure 4 a XPS and **b** FTIR spectra of PMIA, GO and PGAs.

Table 1 Elemental percentages for PGAs from XPS Spectra

Samples	C	O	N
GO powder	71.29	24.42	4.28
PGA-0	81.65	9.93	8.43
PGA-1	77.61	11.96	10.43
PMIA	77.30	12.04	10.66

From the XPS results in Fig. 4a and Table 1, N atom in PGA-0 accounts for 8.43 at. %, almost twice that in GO powder. It confirms the successful introduction of MPD into GO sheets. According to previous studies, doping atoms can damage not only the perfect π-electron conjugation of graphene sheets, but also their crystal structure [31]. The aerogel's thermal conductivity dominated by phonon-phonon interactions therefore will be depressed. That is, due to the introduction of N atoms, thermal insulation ability of PGA-0 was more or less enhanced. Note that, the PGA-0 aerogel used for XPS analysis was the one that went through thermal treatment (230 ^{o}C for 6 h). The above-mentioned value of 8.43 at. % also reveals that the doped N atoms can withstand prolonged exposure to high temperatures up to 230^{o}C. This facilitates PGAs better thermal insulation performance for high temperature applications. As for the supporting polymer PMIA, N atoms and O atoms account for 10.66 at. % and 12.04 at. %, respectively. Since PGA-1 can be considered as a composite product of PGA-0 and PMIA, the elemental percentages of C, N and O atoms within PGA-1 therefore should fall between PGA-0 and PMIA, in accordance with the result in Table 1. The values for C, N and O atoms in PGA-1 were tested to be 77.61 at. %, 11.96 at. % and 10.43 at. %, respectively.

Fig. 4b gives the FTIR spectra of PMIA and related PGAs. It reveals that the interactions among PMIA particles and the MPD doped GO sheets in PGA-1 tend to be physical. As to the prepared PGA-0, the bands observed at the wavenumber of 3444 cm^{-1} and 2922 cm^{-1} represent the stretching vibration of N-H and aromatic C-H groups, respectively. Some other bands located around 1500 cm^{-1} are mainly attributed to the stretching vibration of benzene rings[32]. The successful grafting of MPD onto GO sheets can be confirmed from this. However, the spectra of PGA-1 before and after thermal treatment are very different from that of PGA-0. The characteristic bands observed at 1412 cm^{-1}, 1649 cm^{-1} and 2922 cm^{-1} are assigned to the stretching vibration of aromatic C=C, amide C=O and aromatic C-H groups, respectively [33,34]. The coupled mode of N-H and C-N stretching in C-N-H groups, also known as amide II band, is obtained at 1536 cm^{-1}[35,34]. The broad one centered around 3421 cm^{-1} is attributed to the stretching vibration of N-H and hydrogen bonds between amide groups. These bands are almost the same as the characteristic bands of pure PMIA, but have weaker intensity due to the neutralization of GO sheets. Note that, the band centered around 3421 cm^{-1} seems to have an obvious peak migration. This is caused by the disappearance of a large number of hydrogen bonds as well as the resulting release of N-H in PMIA. Besides, there are also no newly formed bands available. It therefore is believed that the combination of PMIA and the MPD doped GO sheets in PGAs is achieved by physical interactions rather than chemical reactions.

Thermal properties

Thermal conductivity

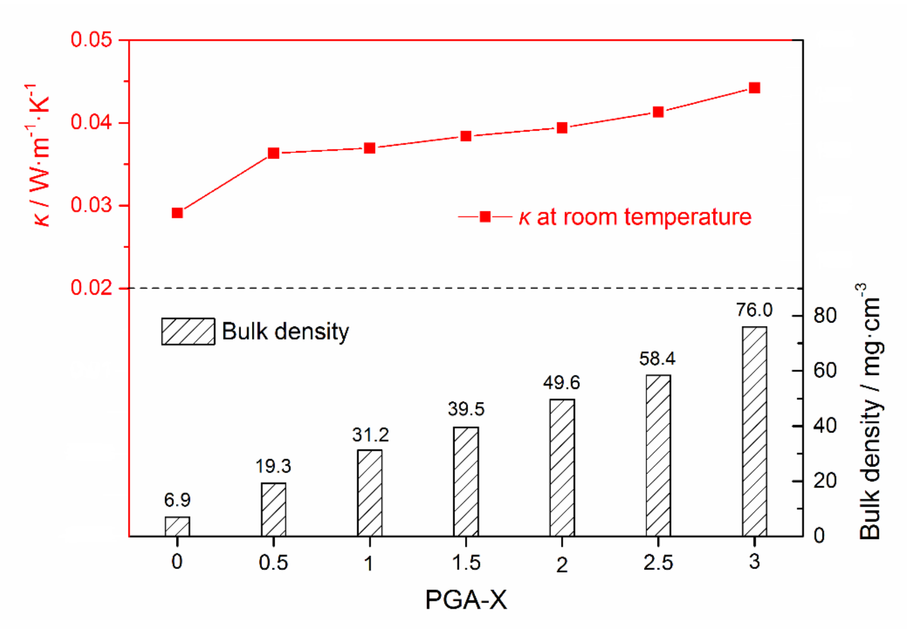

Figure 5 Thermal conductivity (κ) and bulk densities of the prepared PGAs.

It has been widely accepted that graphene aerogels with ultralight bulk density are good insulators for heat transfer [16,36,37,31,38]. Fig. 5 shows the bulk densities and thermal conductivity (κ, at room temperature) of PGAs with different PMIA contents. It is clear that the pristine aerogel with no PMIA incorporated, i.e. PGA-0, had the lowest bulk density and thermal conductivity of 6.9 mg·cm^{-3} and 0.029 W·m^{-1}·K^{-1}, respectively. The value of κ is comparable to that of dry air (κ_{air}=0.027 W·m^{-1}·K^{-1} at 20 °C), indicating that graphene aerogel is indeed one of the ideal materials for thermal insulation. Once PMIA (κ_{PMIA}≈2.4 W·m^{-1}·K^{-1}) was added, the aerogel's bulk density increased gradually, so as the thermal conductivity. Take PGA-0.5 for example, its density and thermal conductivity are about 3 and 1.2 times those of PGA-0, respectively. If the content of PMIA increased further, these two values also increased accordingly. The PGA-3 was calculated to be as high as 76.0 mg·cm^{-3} in density, and at the same time its thermal conductivity increased up to 0.044 W·m^{-1}·K^{-1}. Even so, the prepared composite aerogels in this study are still lightweight and good at thermal insulation, by comparison with the reported ones in Table S1 in the Supplementary Material.

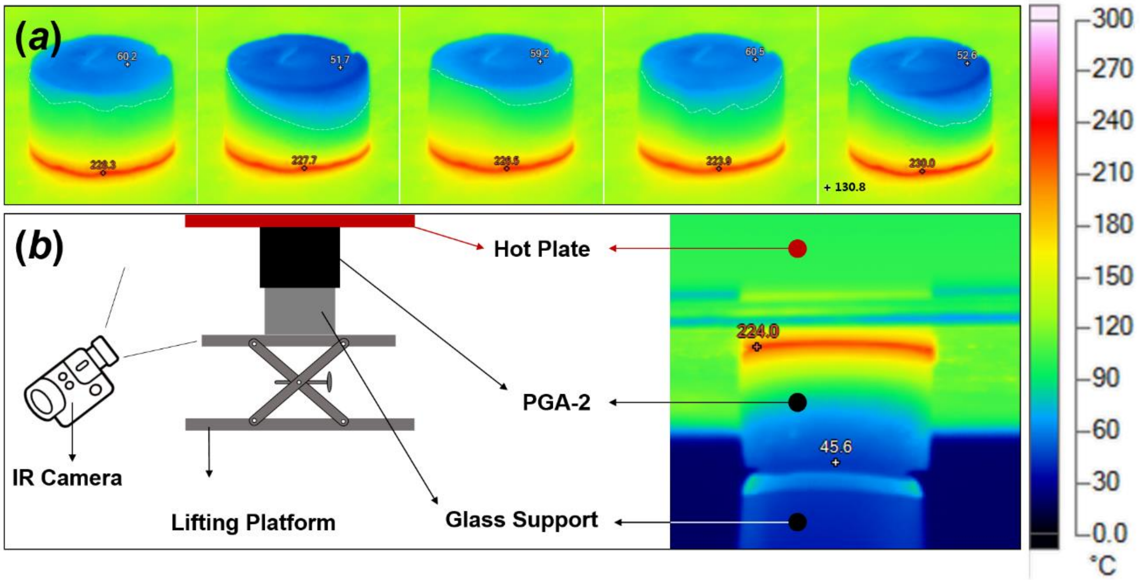

Figure 6 IR images of PGAs-2 placed **a** on and **b** below a hot plate with the temperature of 250°C.

The aerogel's good thermal insulation performance was further verified by using an infrared camera (TiX640, Fluke, USA). At the very beginning, the aerogel was placed on a hot plate facing up. But the results were not satisfactory. The rising hot air during the experiment would always disturb the temperature field around. It therefore would be difficult to obtain a stable thermographic pattern of temperature distribution (see the variable IR images in Fig.6a). Even so, the outer surface temperature of PGAs-2 in Fig.6a was captured to be about 80°C lower than that of the uncovered heat plate, indicating the outstanding heat insulation performance of PGAs-2. To avoid the temperature fluctuation caused by air disturbance, experimental test with the hot plate facing down was then performed as well. The results demonstrated in Fig.6b show that the temperature gradient along the longitudinal direction of the cylindrical aerogel became larger (Δx = 15 mm, $\mathrm{d}T/\mathrm{d}x \approx 12$ °C·mm^{-1}) and more uniform. The energy that flew through the sample thus was estimated to be about 4.7×10^{-4} W·mm^{-2} ($q_{\mathrm{w}} = \kappa\cdot\mathrm{d}T/\mathrm{d}x$), which further reveals that the prepared PGAs possessed good thermal insulation ability. In addition, no apparent loss in aerogel weight (≤±2%) was found before and after the hot plate experiments. This finding agrees well with the TG results in Fig. 7 below. So those results have confirmed that the prepared composite aerogels are suitable for high-temperature insulation applications. Given the long-term working temperature of 220°C for commercial PMIA fibers, however, prolonged exposure to excessive temperatures (>220°C) is not recommended for PGAs.

Thermal decomposition

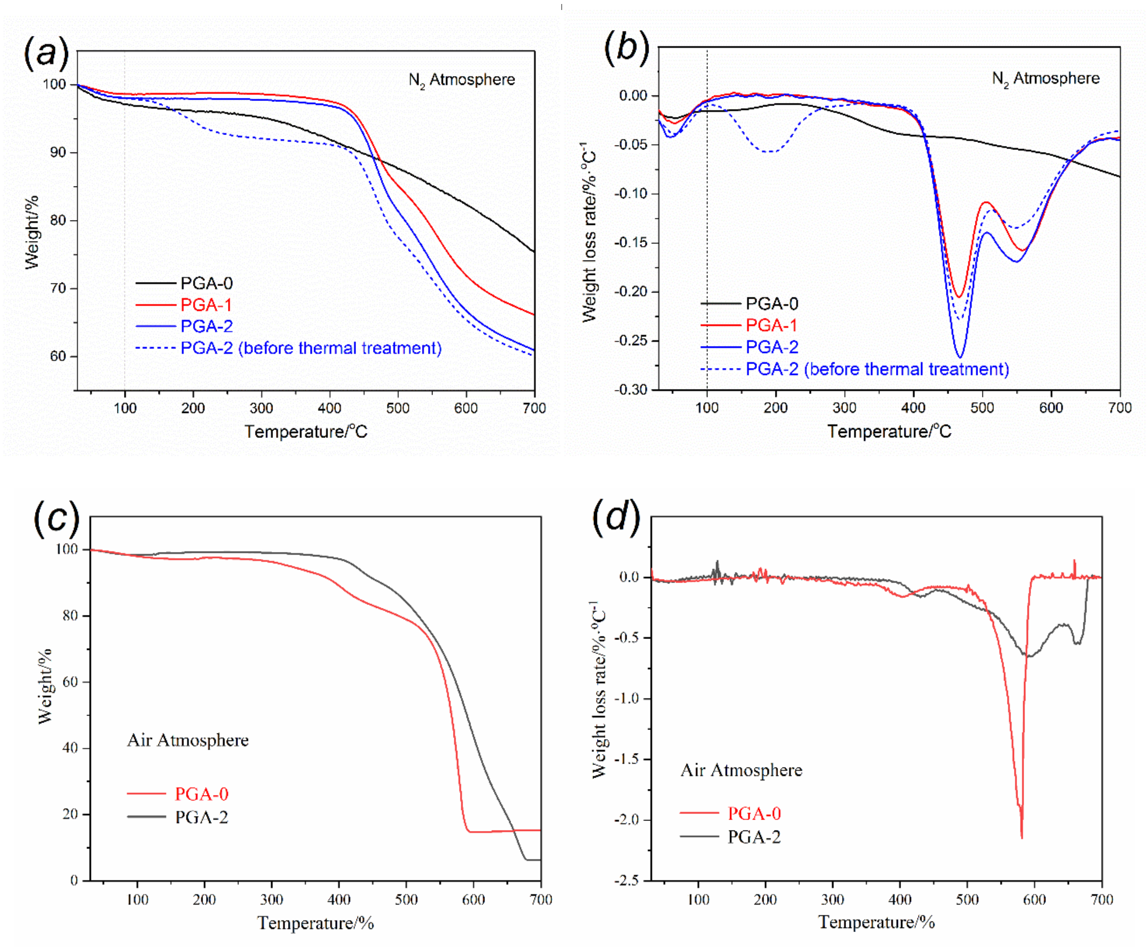

Figure 7 TG and DTG curves of the prepared PGAs: **a** and **b** N_2 atmosphere, **c** and **d** air atmosphere.

Thermal decomposition behavior of the prepared PGAs in nitrogen was studied by a thermo-gravimetric analyzer. The results are plotted in Fig. 7. It is apparent that as-prepared PGA-2 without thermal treatment (230 °C for 6h) show a typical three-step decomposition process. At the very beginning before 100 °C, the sample experienced a gradual weight loss of 7.6%, which can be attributed to the evaporation of moisture and residual solvents. After that, organic branched chains were removed, as shown by an obvious weight loss of 1.2% within 100-400 ^{o}C. The organic branched chains mentioned here refer to oxygen-containing groups on the surface of graphene sheets and their derivatives by reacting with MPD. As the temperature further increased over 400 ^{o}C, PMIA macromolecules began to degrade. This process involved not only polymer rupture but also rearrangement reactions [39,40]. In details, the two weight loss rate peaks observed between 400 ^{o}C and 600 ^{o}C in Fig. 7b correspond to polymer heterolysis and hemolysis, respectively, while the following weight loss over 600 ^{o}C mainly results from dehydrogenation and condensation reactions. The residue that remained at 700 ^{o}C is about 60.1% of its initial mass, indicating good ability to form char.

For the thermal-treated PGA-2, most of its branched chains were removed before TG test. The weight loss steps before 230 ^{o}C thus disappeared, as shown by the blue curve in Fig. 7a. It reveals that thermal treatment resulted in PGAs with better thermal stability. Not only that, at higher temperatures between 230 and 400 ^{o}C, no further weight loss is observed neither. This is owing to the excellent thermal resistance of PMIA. Take the PMIA's long-term working temperature of 220 ^{o}C [41] into consideration, the prepared PGAs can easily survive at such a high temperature. For composite aerogel PGA-1 with less PMIA incorporated, its TG curve maintained a similar trend to that for PGA-2 (the red curve in Fig. 7a). The main difference between them lies in the remaining amount of carbon residue at 700^{o}C, which was mainly caused by the difference in carbon yield rate between PMIA and graphene aerogel. More PMIA contained, less carbon residue remained. From Fig. 7a, carbon residue was found to decrease from 66.2% to 61.0% as the additive amount of PMIA solution increased from 1 g to 2 g. In this case, a higher value (75.4%) for PGA-0 therefore was reasonable. The decomposition of PGA-0, however, was slightly different from others. As the black curve in Fig. 7a shows, PGA-0 went through a gradual weight loss throughout the whole heating process. This is assumed to be the gradual destruction of graphene sheets with N atoms embedded. It is worth noting that a similar weight loss process may also occur to PGA-1 and PGA-2. But their relatively small GO contents made the similar weight loss process less visible.

In addition, thermal decomposition behavior of PGA-0 and PGA-2 in air atmosphere was also conducted. It can be seen from Fig. 7c that PGA-2 has no significant weight loss in the air within 100-400°C, similar to its degradation behavior in nitrogen. But for PGA-0, it still shows a continuous pyrolysis process, especially above 300°C. Once the temperature goes higher than 500°C, the pristine aerogel then suffers a sharp weight loss due to the burning of graphite carbon. The results demonstrate that the weight loss of PGA-2 before 650°C is always lower than that of PGA-0. In other words, the resultant composite aerogel PGA-2 exhibits better thermal stability in air than the pristine PGA-0. This mainly benefit from the inherent flame retardant and heat resistant properties of PMIA, as well as its protective effect on graphene sheets, preventing them from being oxidized by oxygen.

Mechanical Property

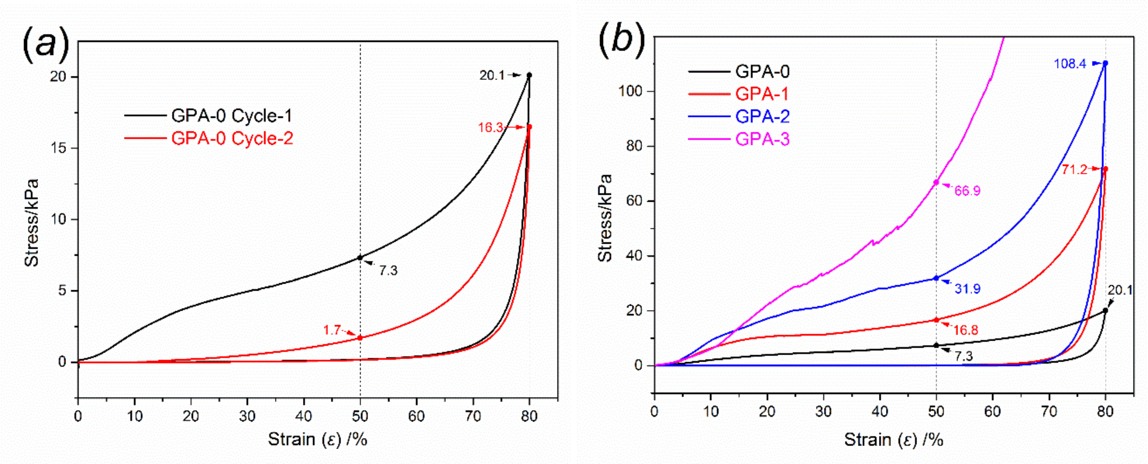

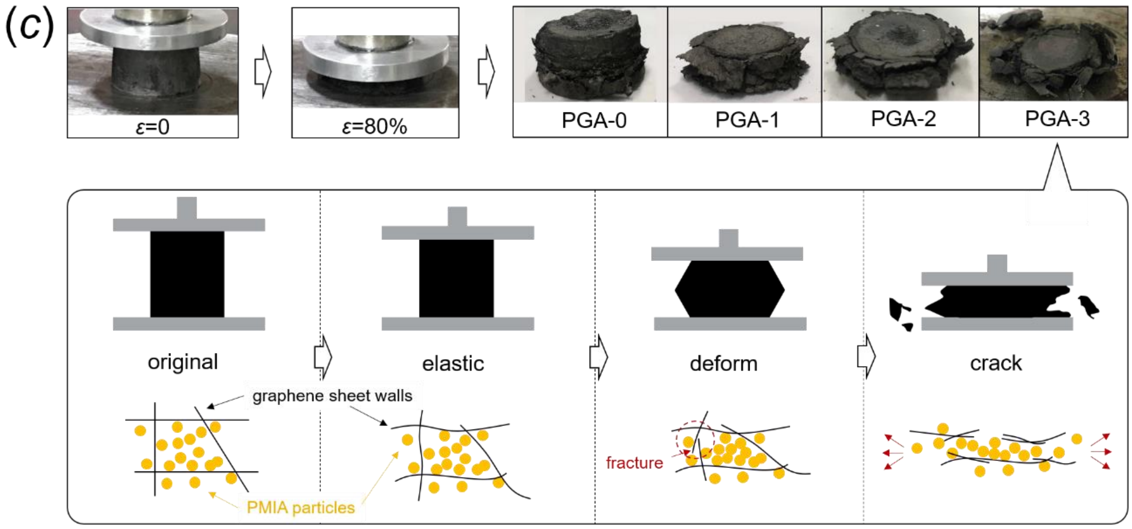

Figure 8 a, b Compressive stress-strain curves of PGAs with a maximum strain of 80%, and **c** their changes in microstructure and appearance during compression.

The compressive stress-strain curves of PGAs with a maximum strain of 80 % are presented in Fig. 8. Experimental results indicate that the pristine graphene aerogel without PMIA (i.e. PGA-0) can be easily compressed into a thin “pancake”. As the black curve in Fig. 8a shows, the first loading process of PGA-0 was observed to have three regions [19,42]. Among them, the first one at about ε < 10 % was known as the elastic region, in which stress increased almost linearly with strain. After that, the stress increased slowly as the absorbed energy dissipated, indicative of reaching a plateau region. If the strain increased above 60%, a densification region resulting from decreasing pore volume then appeared. The stress at 50 % and 80 % strain for PGA-0 in the first loading process were tested to be 7.3 kPa and 20.1 kPa, respectively. While for the second compression cycle, the hysteresis loop was much narrower. The stress appearing at 50 % and 80 % strain were 5.6 kPa and 3.7 kPa lower than those of the first cycle. The difference should be mainly attributed to the permanent structural deformation caused by compression. Also because of this, the compressed “pancake” could no longer recover to their original structure but to a deformed dwarf cylinder with many surface wrinkles (see Fig. 8c). In other words, GPA-0 was compressible and can be partially restored after compression stress was removed.

When it came to the PMIA-containing GPAs, their compressive strengths were greatly improved. The stress values for GPA-1 and GPA-3 at 50 % strain were tested to be

16.8 kPa and 66.9 kPa, respectively, about 2 and 9 times that of GPA-0. This improvement is mainly due to the supporting and gluing effects of PMIA. The supporting effect mentioned here results from the filling of PMIA particles and the resulting increase in aerogel density, while the gluing effect mainly refers to the bridging of graphene sheets by PMIA particles. For GPA-1 with relatively low PMIA content incorporated, its morphology in Fig. 2b didn't change much compared to GPA-0. The difference between them was mainly in pore size and the thickness of graphene sheet walls. Besides, GPA-2 and GPA-3 with more PMIA incorporated could easily withstand greater stress. Fig. 1 shows that a 0.23 g composite aerogel GPA-2 could easily support a 500 g counterpoise, more than 2000 times its own weight. This is living proof of the excellent mechanical property of GPA-2, i.e. enhanced shape stability. To be honest, there were also some other reports of more robust graphene-based composite aerogels, especially those reduced by L-ascorbic acid or reinforced by carbon nanotubes[43,44]. But from the aspects of economy, high temperature resistance, heat insulation, etc., the GPAs prepared in this study are still attractive.

From above discussions, it has become apparent that higher PMIA content corresponds to better strength but less flexibility. Given their difference in density, PGAs with higher PMIA content may undergo more severe radial expansion. The images in Fig. 8c illustrate the changes in microstructure and appearance of PGA-3 during compression. At the very beginning, PGA-3 will keep its original shape without deformation. This is also due to the supporting effects of the pore walls and some PMIA particles. If the external stress increases beyond a certain value, PGA-3 begins to shrink and can be recovered with stress removed. It likes an elastomer in this stage, but the duration is very short. As the strain increases further, the pores inside PGA-3 continue to deform. Large-scale microstructure fracture, such as wall collapse, etc., then takes place continuously to dissipate the accumulated energy, and results in visible but irreversible shape changes. However, this is not the final form. More severe strain will further cause the composite aerogel to crack. The densification of PMIA particles and graphene sheets should be the main reasons. As a result, the aerogel PGA-3 was pressed into a "pancake" with a few fragments scattered around.

Conclusions

In this study, PMIA with excellent thermal resistant and flame retardant properties was used as the supporting material for developing graphene aerogels with improved compressive shape stability at high temperatures. These composite aerogels were prepared by premixing a certain amount of PMIA in GO suspension, followed by a classical freeze-drying process. Experimental results have revealed that the PMIA incorporated appeared as micro particles that filled in the pores of aerogel, resulting in denser composites with smaller pore size and thinner walls. These particles formed attach themselves to each other and to the surface of graphene sheets, and therefore hindered the stacking of graphene sheets in the process of self-assembly as well as practical compression. As a result, the compressive strength of PGAs was dramatically enhanced. The resultant composite aerogel can easily support a counterpoise of more than 2000 times its own weight without visible deformation. Besides, the thermal conductivity test of the prepared aerogels has demonstrated that PGAs suffered a gradual degradation in thermal insulation as PMIA content increases, but still maintained good thermal insulator with thermal conductivity less than 0.045 $W \cdot m^{-1} \cdot K^{-1}$. Since the supporting polymer PMIA could survive prolonged applications up to 220^{o}C, the developed composite aerogels with better compressive shape stability and considerable thermal insulation may be an excellent candidate for a wide range of high-temperature applications.

Acknowledgements

This work was supported by National Natural Science Foundation of China (Grant No. 51904312), Shandong “Taishan Youth Scholar Program” and Research Start-up Funds of Civil Aviation University of China (600005140216). The authors are deeply grateful to these supports.

Compliance with ethical standards

Conflicts of interest: The author declares no conflict of interest.

References

1. Le DK, Ng GN, Koh HW, Zhang X, Thai QB, Phan-Thien N, Duong HM (2020) Methyltrimethoxysilane-coated recycled polyethylene terephthalate aerogels for oil spill cleaning applications. Mater Chem Phys 239:122064. doi:https://doi.org/10.1016/j.matchemphys.2019.122064
2. Kashyap S, Kabra S, Kandasubramanian B (2020) Graphene aerogel-based phase changing composites for thermal energy storage systems. J Mater Sci 55 (10):4127-4156. doi:https://doi.org/10.1007/s10853-019-04325-7
3. Wang J, Liu D, Li Q, Chen C, Chen Z, Song P, Hao J, Li Y, Fakhrhoseini S, Naebe M, Wang X, Lei W (2019) Lightweight, superelastic yet thermoconductive boron nitride nanocomposite aerogel for thermal energy regulation. ACS Nano 13 (7):7860-7870. doi:https://doi.org/10.1021/acsnano.9b02182
4. Maleki H, Hüsing N (2018) Current status, opportunities and challenges in catalytic and photocatalytic applications of aerogels: Environmental protection aspects. Appl Catal B: Environ 221:530-555. doi:https://doi.org/10.1016/j.apcatb.2017.08.012
5. Stergar J, Maver U (2016) Review of aerogel-based materials in biomedical applications. J Sol-Gel Sci Techn 77 (3):738-752. doi:https://doi.org/10.1007/s10971-016-3968-5
6. Hasan MA, Sangashetty R, Esther ACM, Patil SB, Sherikar BN, Dey A (2017) Prospect of thermal insulation by silica aerogel: A brief review. J I Eng (India): Ser D 98 (2):297-304. doi:https://doi.org/10.1007/s40033-017-0136-1
7. Hu L, He R, Lei H, Fang D (2019) Carbon aerogel for insulation applications: A review. Int J Thermophys 40 (4):39. doi:https://doi.org/10.1007/s10765-019-2505-5
8. Benad A, Jürries F, Vetter B, Klemmed B, Hübner R, Leyens C, Eychmüller A (2018) Mechanical properties of metal oxide aerogels. Chem Mater 30 (1):145-152. doi:https://doi.org/10.1021/acs.chemmater.7b03911
9. Yang Z, Yu H, Li X, Ding H, Ji H (2019) Hyperelastic and hydrophobic silica aerogels with enhanced compressive strength by using VTES/MTMS as precursors. Journal of Non-Crystalline Solids 525:119677. doi:10.1016/j.jnoncrysol.2019.119677
10. Gorgolis G, Galiotis C (2017) Graphene aerogels: A review. 2D Mater 4 (3):032001. doi:https://doi.org/10.1088/2053-1583/aa7883
11. Lorenzetti A, Roso M, Bruschetta A, Boaretti C, Modesti M (2016) Polyurethane-graphene nanocomposite foams with enhanced thermal insulating properties. Polym Adv Technol 27 (3):303-307. doi:https://doi.org/10.1002/pat.3635
12. Korkmaz S, Kariper İA (2020) Graphene and graphene oxide based aerogels: Synthesis, characteristics and supercapacitor applications. J Energy Storage 27:101038. doi:https://doi.org/10.1016/j.est.2019.101038

13. Liao H, Chen W, Liu Y, Wang Q (2020) A phase change material encapsulated in a mechanically strong graphene aerogel with high thermal conductivity and excellent shape stability. Compos Sci Technol 189:108010. doi:https://doi.org/10.1016/j.compscitech.2020.108010
14. Wu H, Wang Z-M, Kumagai A, Endo T (2019) Amphiphilic cellulose nanofiber-interwoven graphene aerogel monolith for dyes and silicon oil removal. Compos Sci Technol 171:190-198. doi:https://doi.org/10.1016/j.compscitech.2018.12.017
15. Huang H, Chen P, Zhang X, Lu Y, Zhan W (2013) Edge-to-edge assembled graphene oxide aerogels with outstanding mechanical performance and superhigh chemical activity. Small 9 (8):1397-1404. doi:https://doi.org/10.1002/smll.201202965
16. Yue C, Feng J, Feng J, Jiang Y (2017) Ultralow-density and high-strength graphene aerogels composites for thermal insulation. Mater Lett 188:169-171. doi:https://doi.org/10.1016/j.matlet.2016.11.028
17. Ha H, Shanmuganathan K, Ellison CJ (2015) Mechanically stable thermally crosslinked poly(acrylic acid)/reduced graphene oxide aerogels. ACS Appl Mater Inter 7 (11):6220-6229. doi:https://doi.org/10.1021/acsami.5b00407
18. Lu H, Li C, Zhang B, Qiao X, Liu C (2016) Toward highly compressible graphene aerogels of enhanced mechanical performance with polymer. RSC Adv 6 (49):43007-43015. doi:https://doi.org/10.1039/c6ra04995h
19. Qin Y, Peng Q, Ding Y, Lin Z, Wang C, Li Y, Xu F, Li J, Yuan Y, He X, Li Y (2015) Lightweight, superelastic, and mechanically flexible graphene/polyimide nanocomposite foam for strain sensor application. ACS Nano 9 (9):8933-8941. doi:https://doi.org/10.1021/acsnano.5b02781
20. Ren R, Wang Z, Ren J, Lv Y (2019) Highly compressible polyimide/graphene aerogel for efficient oil/water separation. J Mater Sci 54 (7):5918-5926. doi:https://doi.org/10.1007/s10853-018-03238-1
21. Ye S, Feng J (2014) Towards three-dimensional, multi-functional graphene-based nanocomposite aerogels by hydrophobicity-driven absorption. J Mater Chem A 2 (27):10365-10369. doi:https://doi.org/10.1039/c4ta01392a
22. Hu H, Zhao Z, Wan W, Gogotsi Y, Qiu J (2014) Polymer/graphene hybrid aerogel with high compressibility, conductivity, and “sticky” superhydrophobicity. ACS Appl Mater Inter 6 (5):3242-3249. doi:https://doi.org/10.1021/am4050647
23. García JM, García FC, Serna F, de la Peña JL (2010) High-performance aromatic polyamides. Prog Polym Sci 35 (5):623-686. doi:https://doi.org/10.1016/j.progpolymsci.2009.09.002
24. Chen W, Weng W (2016) Ultrafine lauric-myristic acid eutectic/poly (meta-phenylene isophthalamide) form-stable phase change fibers for thermal energy storage by electrospinning. Appl Energ 173:168-176. doi:https://doi.org/10.1016/j.apenergy.2016.04.061

25. Zhang Q, Xu X, Lin D, Chen W, Xiong G, Yu Y, Fisher TS, Li H (2016) Hyperbolically patterned 3D graphene metamaterial with negative poisson's ratio and superelasticity. Adv mater 28 (11):2229-2237. doi:https://doi.org/10.1002/adma.201505409
26. Qiu L, Liu JZ, Chang SLY, Wu Y, Li D (2012) Biomimetic superelastic graphene-based cellular monoliths. Nat Commun 3 (1):1241. doi:https://doi.org/10.1038/ncomms2251
27. Adhikari B, Biswas A, Banerjee A (2012) Graphene oxide-based hydrogels to make metal nanoparticle-containing reduced graphene oxide-based functional hybrid hydrogels. ACS Appl Mater Inter 4 (10):5472-5482. doi:https://doi.org/10.1021/am301373n
28. Wang J, Ellsworth M (2009) Graphene aerogels. ECS Trans 19 (5):241-247. doi:https://doi.org/10.1149/1.3119548
29. Yao L, Lee C, Kim J (2010) Fabrication of electrospun meta-aramid nanofibers in different solvent systems. Fibers and Polymers 11 (7):1032-1040. doi:10.1007/s12221-010-1032-6
30. Maleki H, Durães L, Portugal A (2014) An overview on silica aerogels synthesis and different mechanical reinforcing strategies. J Non-Cryst Solids 385:55-74. doi:https://doi.org/10.1016/j.jnoncrysol.2013.10.017
31. Yue C, Feng J, Feng J, Jiang Y (2016) Low-thermal-conductivity nitrogen-doped graphene aerogels for thermal insulation. RSC Adv 6 (12):9396-9401. doi:https://doi.org/10.1039/c5ra23236h
32. Lu Y, Zhang F, Zhang T, Leng K, Zhang L, Yang X, Ma Y, Huang Y, Zhang M, Chen Y (2013) Synthesis and supercapacitor performance studies of N-doped graphene materials using o-phenylenediamine as the double-N precursor. Carbon 63:508-516. doi:https://doi.org/10.1016/j.carbon.2013.07.026
33. Wang T, He X, Li Y, Li J (2018) Novel poly(piperazine-amide) (PA) nanofiltration membrane based poly(m -phenylene isophthalamide) (PMIA) hollow fiber substrate for treatment of dye solutions. Chemical Engineering Journal 351. doi:10.1016/j.cej.2018.06.165
34. Pramila J, Melbiah JSB, Rana D, Gandhi NN, Nagendran A, Mohan D (2018) Permeation characteristics of tailored poly (m-phenylene isophthalamide) ultrafiltration membranes and probing its efficacy on bovine serum albumin separation. Polymer Testing 67:218-227. doi:https://doi.org/10.1016/j.polymertesting.2018.03.006
35. Lee JW, Han SS, Zo SM, Choi SM (2018) Cellulose/poly-(m-phenylene isophthalamide) porous film as a tissue-engineered skin bioconstruct. Results in Physics 9:113-120. doi:https://doi.org/10.1016/j.rinp.2018.02.003
36. Zhang Q, Hao M, Xu X, Xiong G, Li H, Fisher TS (2017) Flyweight 3D graphene scaffolds with microinterface barrier-derived tunable thermal insulation and flame retardancy. ACS Appl Mater Inter 9 (16):14232-14241. doi:https://doi.org/10.1021/acsami.7b01697

37. Cheng Y, Zhou S, Hu P, Zhao G, Li Y, Zhang X, Han W (2017) Enhanced mechanical, thermal, and electric properties of graphene aerogels via supercritical ethanol drying and high-temperature thermal reduction. Sci Rep 7 (1):1439. doi:https://doi.org/10.1038/s41598-017-01601-x
38. Kim WS, Moon SY, Koyanagi J, Ogasawara T (2016) Three-dimensional porous graphene-based ultra-lightweight aerofoam exhibiting good thermal insulation. Adv Compos Mater 25 (sup1):105-113. doi:https://doi.org/10.1080/09243046.2016.1193939
39. Villar-Rodil S, Martínez-Alonso A, Tascón JMD (2001) Studies on pyrolysis of Nomex polyaramid fibers. J Anal Appl Pyrol 58-59:105-115. doi:https://doi.org/10.1016/S0165-2370(00)00124-8
40. Villar-Rodil S, Paredes JI, Martínez-Alonso A, Tascón JMD (2001) Atomic force microscopy and infrared spectroscopy studies of the thermal degradation of nomex aramid fibers. Chem Mater 13 (11):4297-4304. doi:https://doi.org/10.1021/cm001219f
41. Deoghare RR, Sirsat PM, Tamboli RA (2014) Design and analysis of pressure disc type filter for beverages making equipment manufacturer. Int J Eng Sci Res Technol 3 (4):2014-2017. doi:http://www.ijesrt.com/issues%20pdf%20file/Archives-2014/April-2014/38.pdf
42. Zhu C, Han TY-J, Duoss EB, Golobic AM, Kuntz JD, Spadaccini CM, Worsley MA (2015) Highly compressible 3D periodic graphene aerogel microlattices. Nat Commu 6 (1):6962. doi:https://doi.org/10.1038/ncomms7962
43. Zhang X, Sui Z, Xu B, Yue S, Luo Y, Zhan W, Liu B (2011) Mechanically strong and highly conductive graphene aerogel and its use as electrodes for electrochemical power sources. Journal of Materials Chemistry 21 (18):6494-6497. doi:10.1039/C1JM10239G
44. Guo K, Hu Z, Song H, Du X, Zhong L, Chen X (2015) Low-density graphene/carbon composite aerogels prepared at ambient pressure with high mechanical strength and low thermal conductivity. RSC Advances 5 (7):5197-5204. doi:10.1039/C4RA08800J

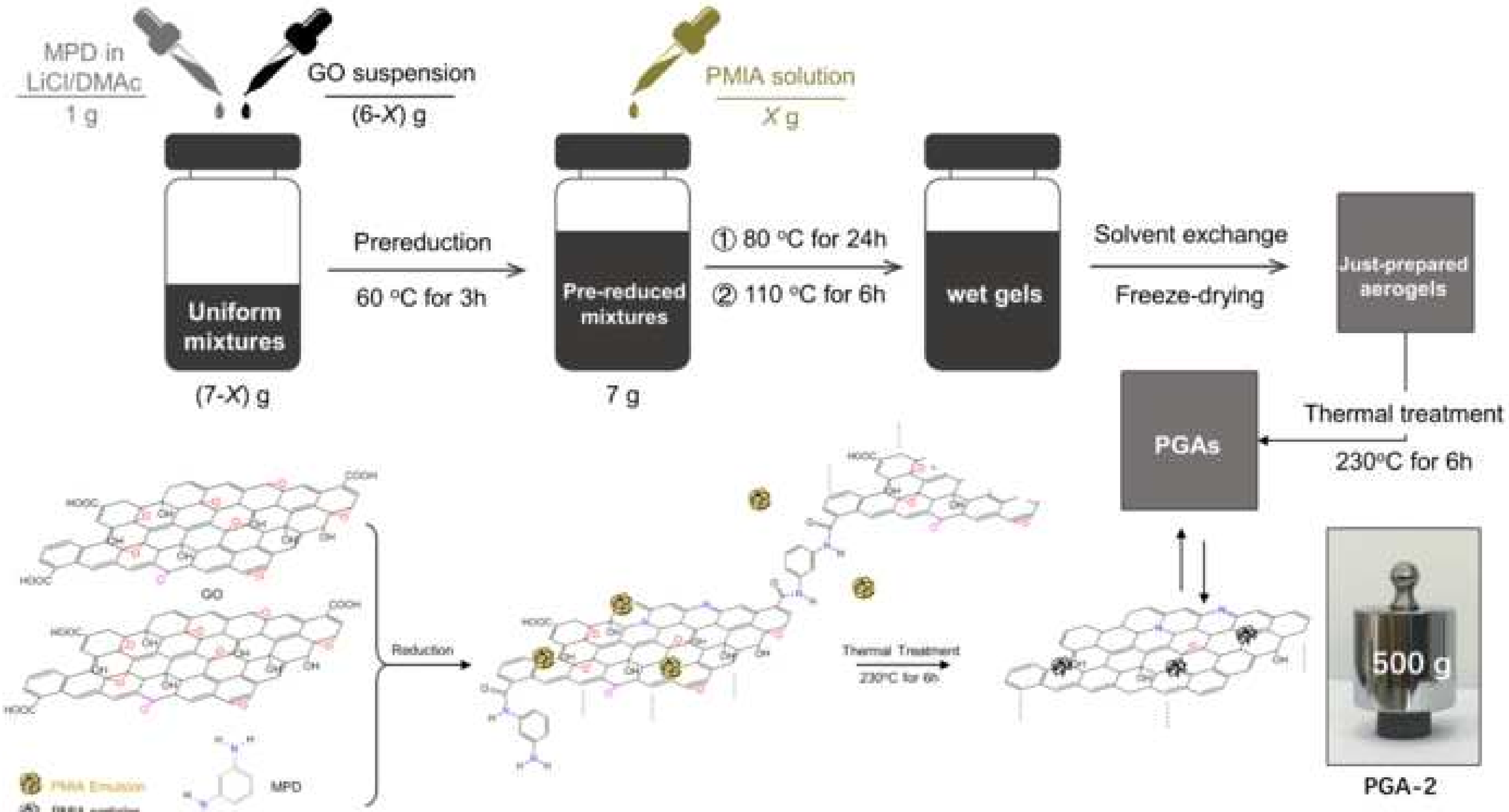
MPD in LiCl/DMAc
1 g
GO suspension
(6-*X*) g
Uniform mixtures
(7-*X*) g
Prereduction
60 °C for 3h
Pre-reduced mixtures
7 g
PMIA solution
X g
① 80 °C for 24h
② 110 °C for 6h
wet gels
Solvent exchange
Freeze-drying
Just-prepared aerogels
Thermal treatment
230°C for 6h
PGAs
GO
HOOC
COOH
OH
Reduction
Thermal Treatment
230°C for 6h
PMIA Emulsion
PMIA particles
MPD
500 g
PGA-2

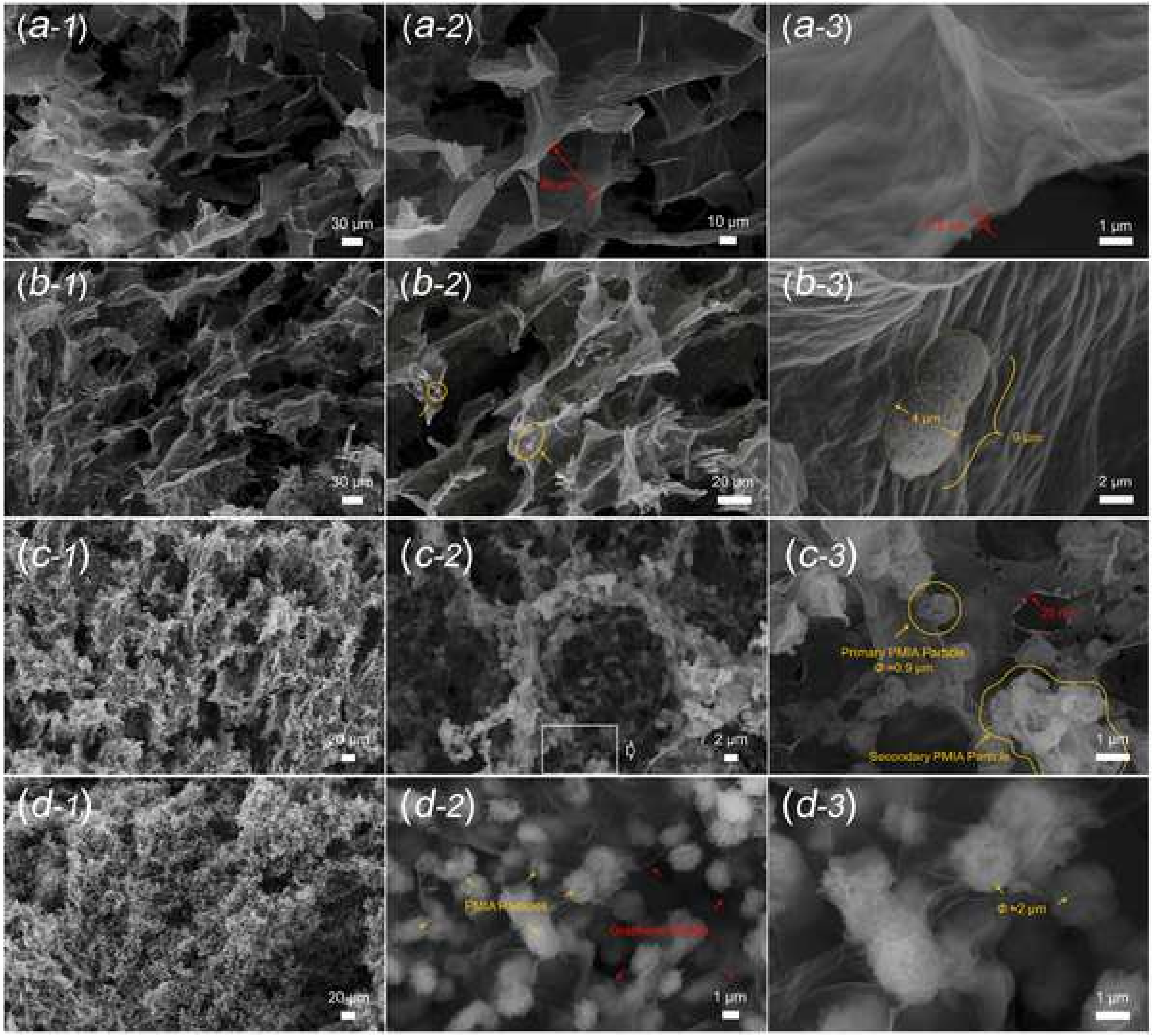
(a-1)
30 μm
(a-2)
10 μm
(a-3)
1 μm
(b-1)
30 μm
(b-2)
20 μm
(b-3)
4 μm
9 μm
2 μm
(c-1)
20 μm
(c-2)
2 μm
(c-3)
Primary PMIA Particle
Φ ≈0.9 μm
Secondary PMIA Particle
1 μm
(d-1)
20 μm
(d-2)
PMIA Particles
1 μm
(d-3)
Φ ≈2 μm
1 μm

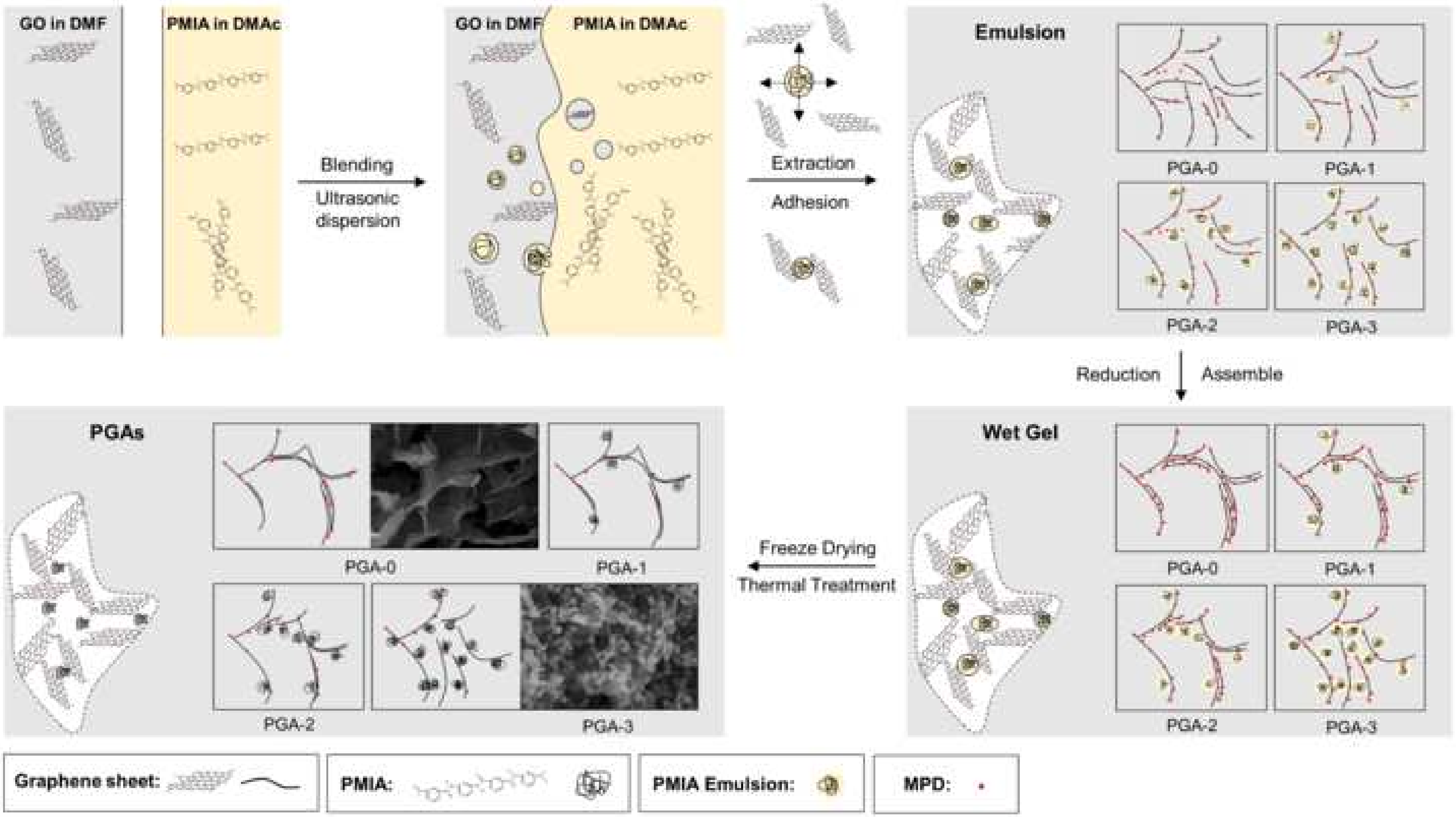
GO in DMF
PMIA in DMAc
Blending
Ultrasonic dispersion
GO in DMF
PMIA in DMAc
Extraction
Adhesion
Emulsion
PGA-0
PGA-1
PGA-2
PGA-3
Reduction
Assemble
Wet Gel
PGA-0
PGA-1
PGA-2
PGA-3
Freeze Drying
Thermal Treatment
PGAs
PGA-0
PGA-1
PGA-2
PGA-3
Graphene sheet:
PMIA:
PMIA Emulsion:
MPD:

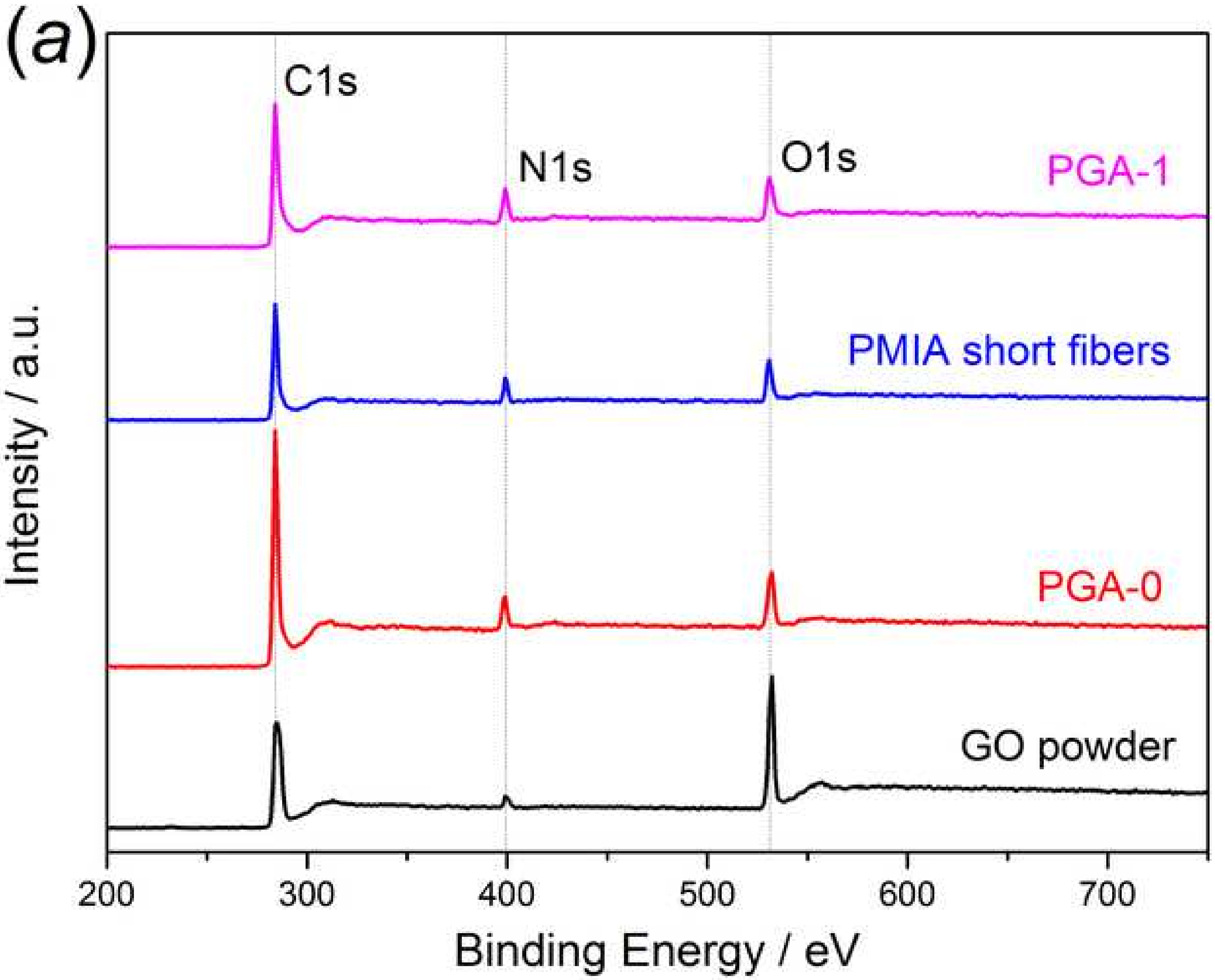
(a)
C1s
N1s
O1s
PGA-1
PMIA short fibers
PGA-0
GO powder
Intensity / a.u.
200
300
400
500
600
700
Binding Energy / eV

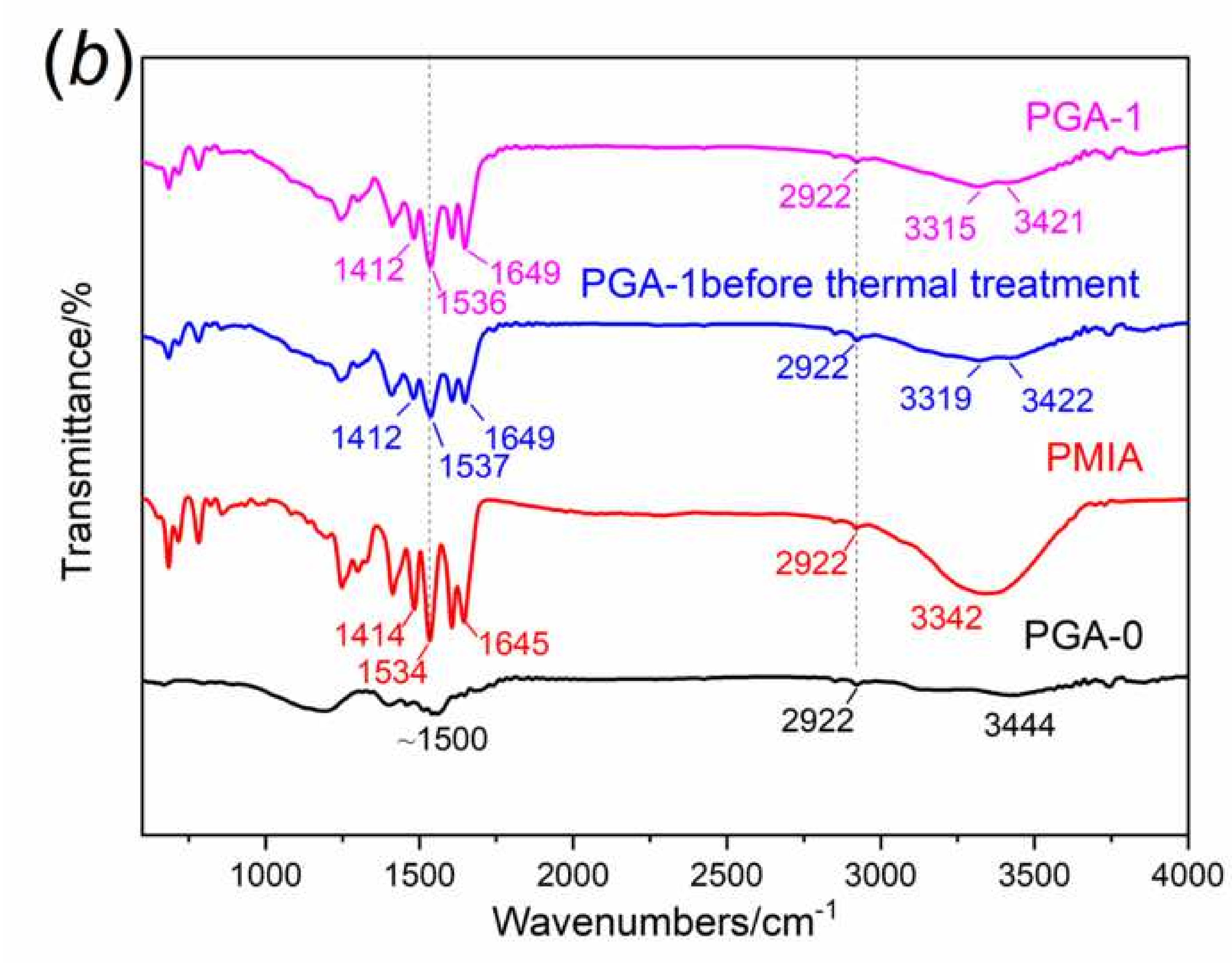
(b)
PGA-1
2922
3315
3421
1412
1536
1649
PGA-1before thermal treatment
2922
3319
3422
1412
1537
1649
PMIA
2922
3342
1414
1534
1645
PGA-0
2922
3444
~1500
Transmittance/%
1000
1500
2000
2500
3000
3500
4000
Wavenumbers/cm-1

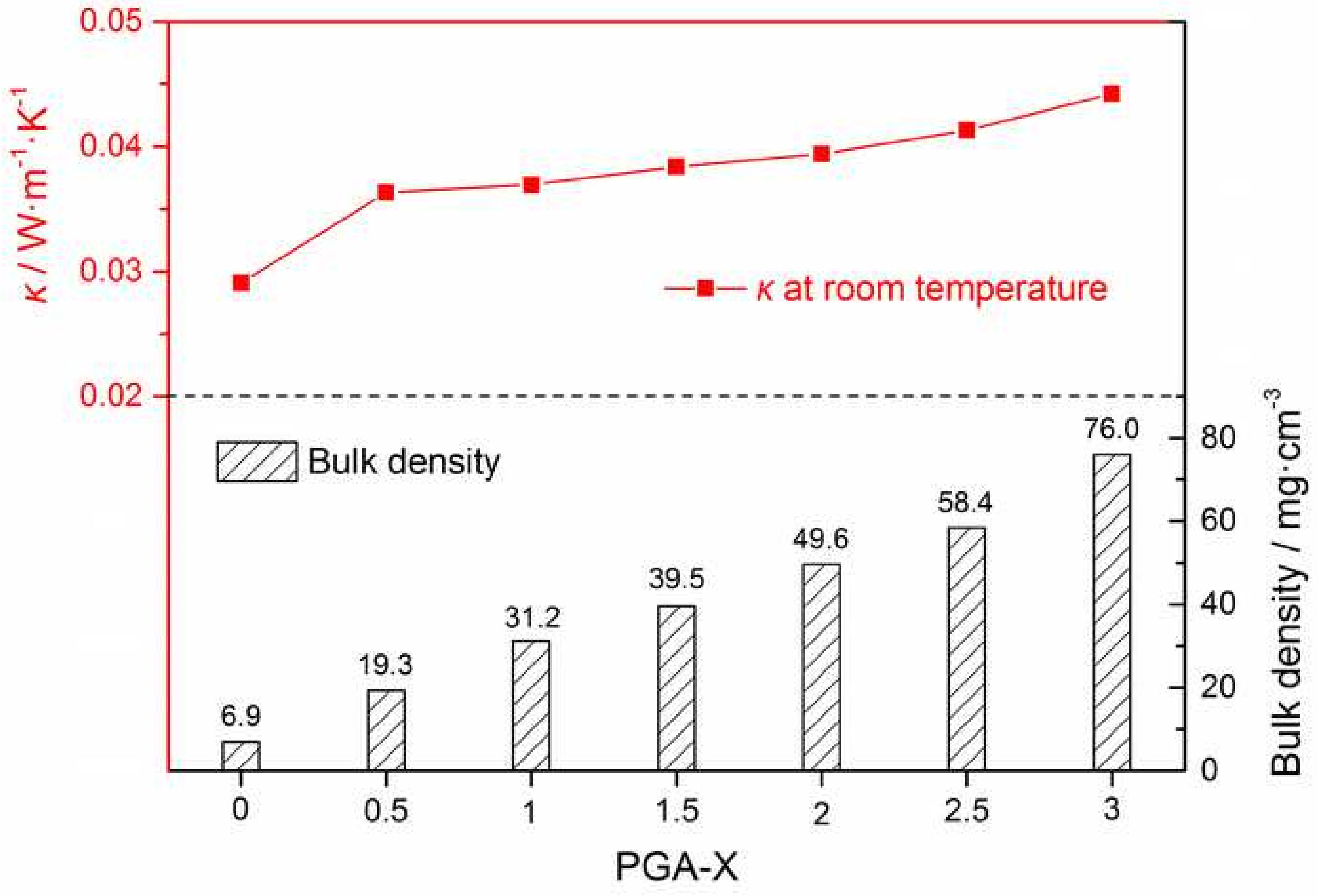
0.05
0.04
0.03
0.02
κ / W·m⁻¹·K⁻¹
κ at room temperature
Bulk density
6.9
19.3
31.2
39.5
49.6
58.4
76.0
0
20
40
60
80
Bulk density / mg·cm⁻³
0
0.5
1
1.5
2
2.5
3
PGA-X

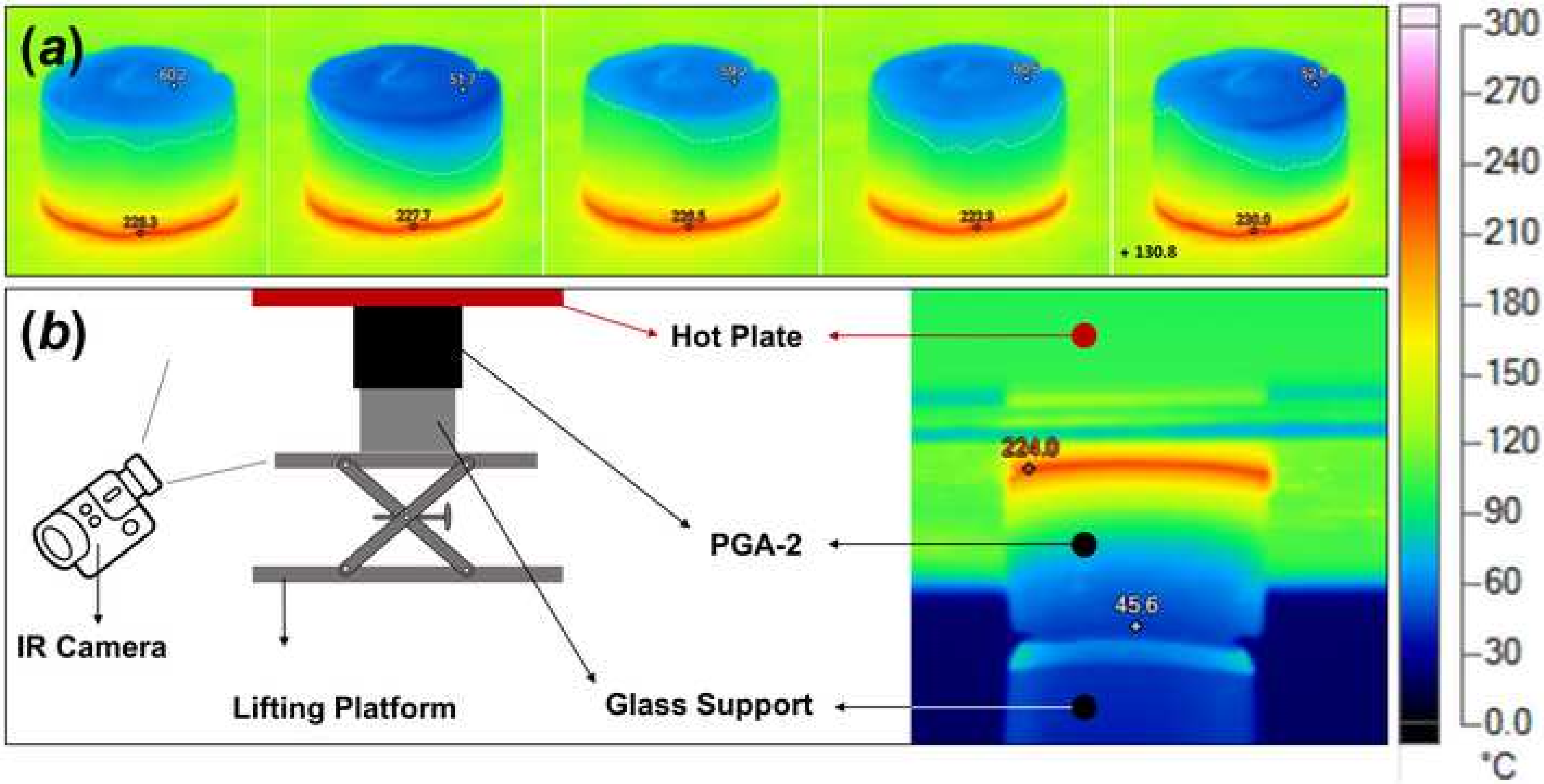
(a)
60.2
51.7
228.3
227.7
228.5
223.8
230.0
+ 130.8
(b)
Hot Plate
PGA-2
IR Camera
Lifting Platform
Glass Support
224.0
45.6
300
270
240
210
180
150
120
90
60
30
0.0
°C

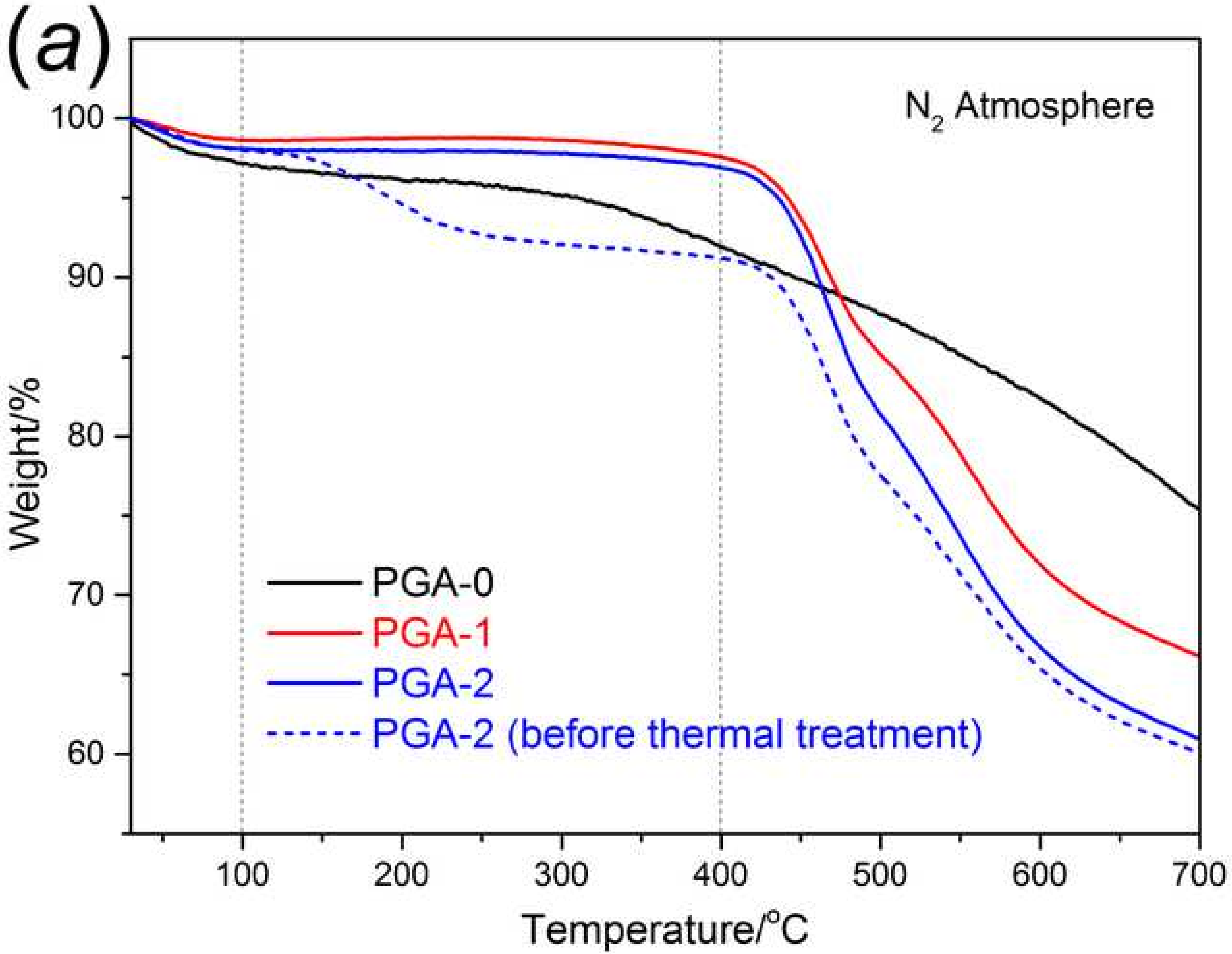
(a)
N$_2$ Atmosphere
Weight/%
100
90
80
70
60
100
200
300
400
500
600
700
Temperature/°C
PGA-0
PGA-1
PGA-2
PGA-2 (before thermal treatment)

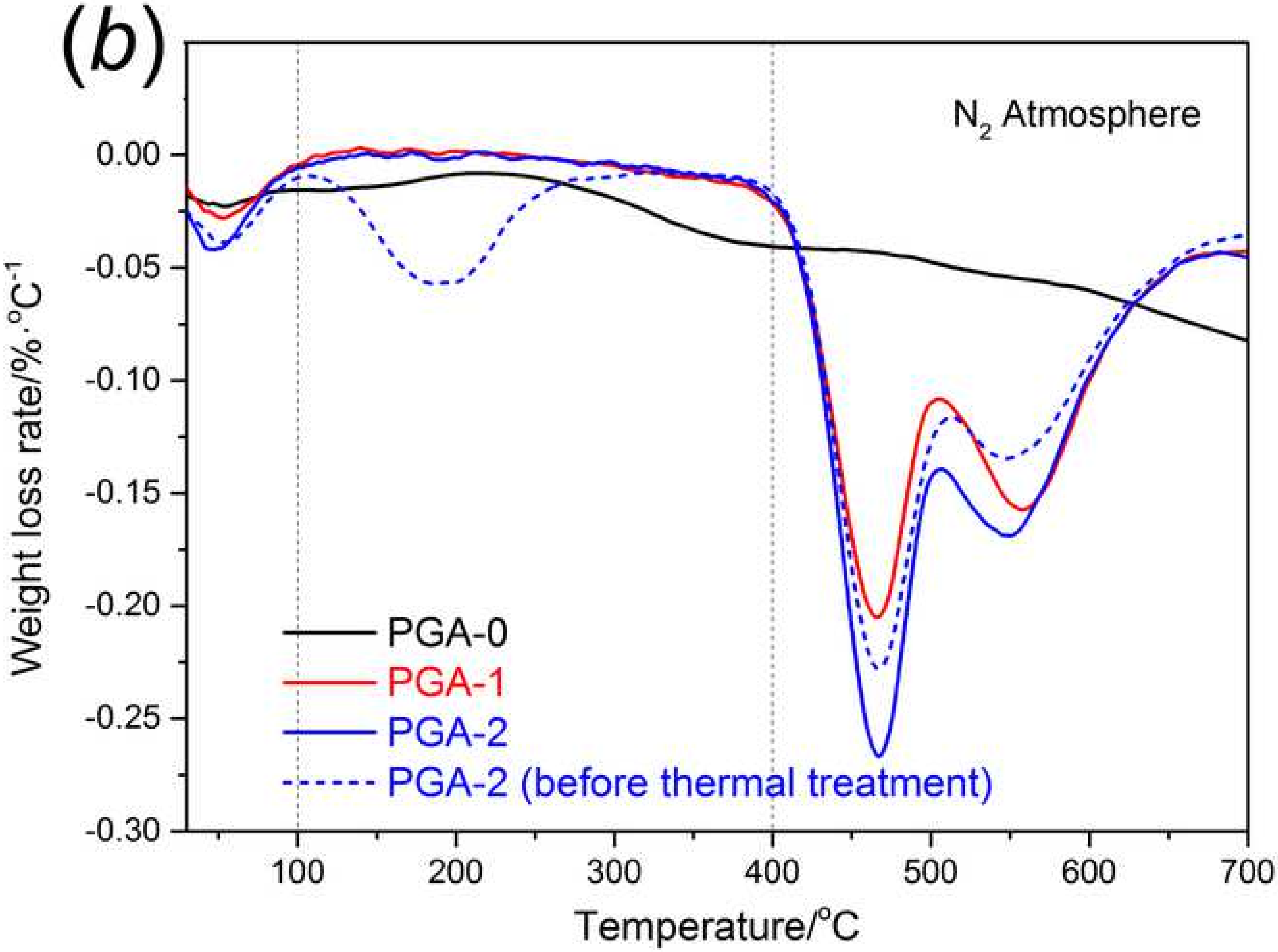
(b)
N₂ Atmosphere
Weight loss rate/%·°C⁻¹
0.00
-0.05
-0.10
-0.15
-0.20
-0.25
-0.30
100
200
300
400
500
600
700
Temperature/°C
PGA-0
PGA-1
PGA-2
PGA-2 (before thermal treatment)

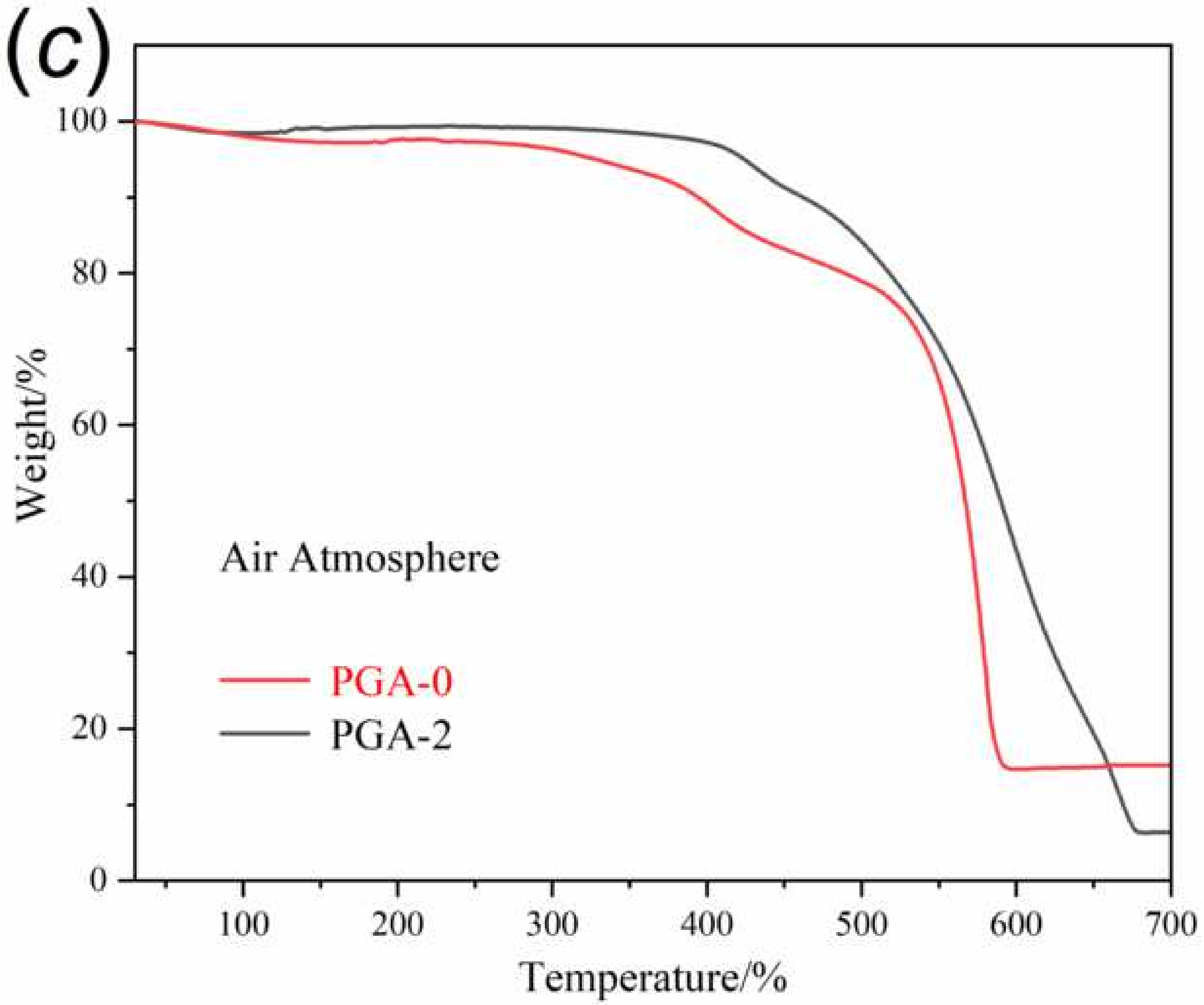
(c)
Weight/%
100
80
60
40
20
0
100
200
300
400
500
600
700
Temperature/%
Air Atmosphere
PGA-0
PGA-2

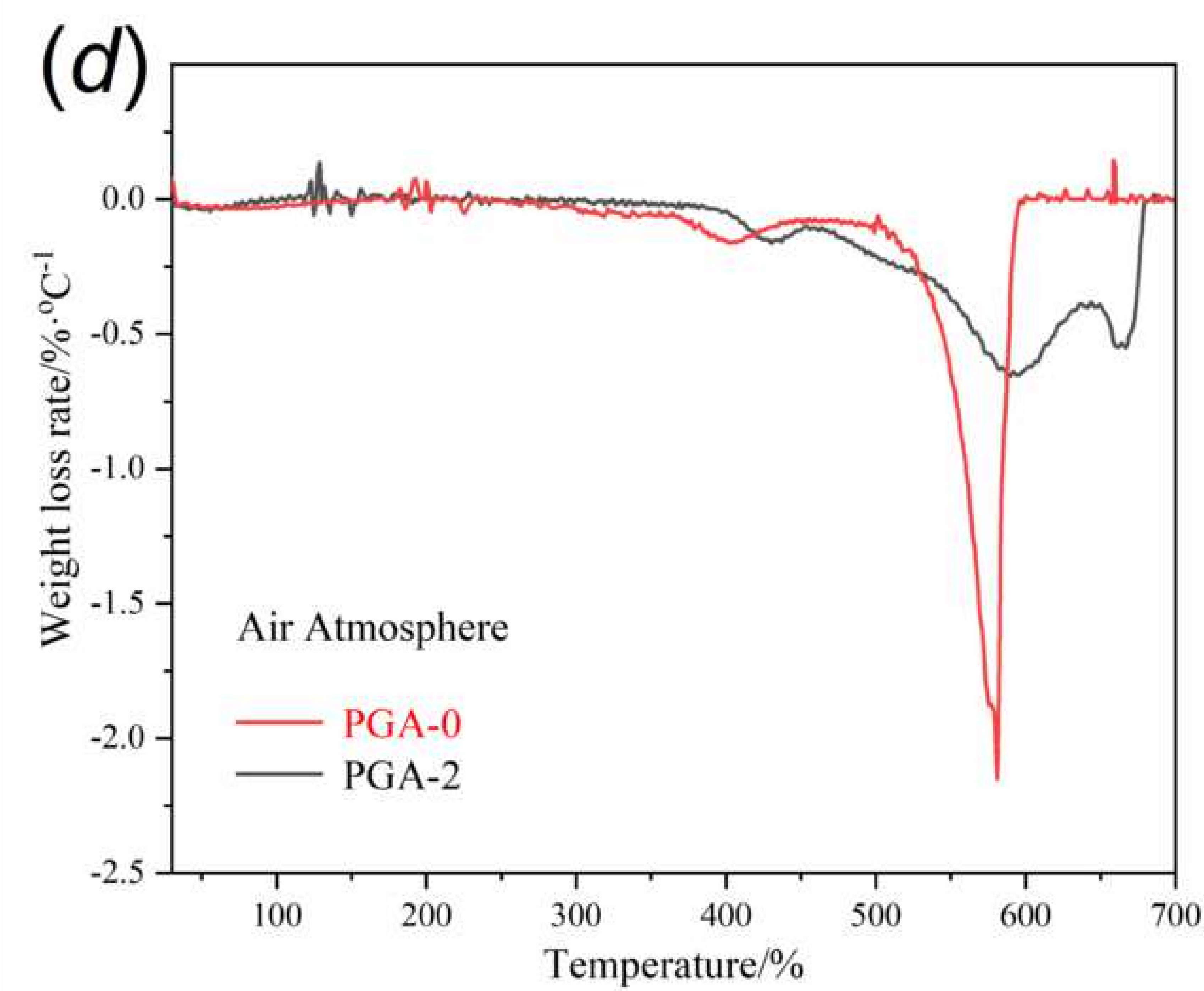
(d)
Weight loss rate/%·°C⁻¹
0.0
-0.5
-1.0
-1.5
-2.0
-2.5
100
200
300
400
500
600
700
Temperature/%
Air Atmosphere
PGA-0
PGA-2

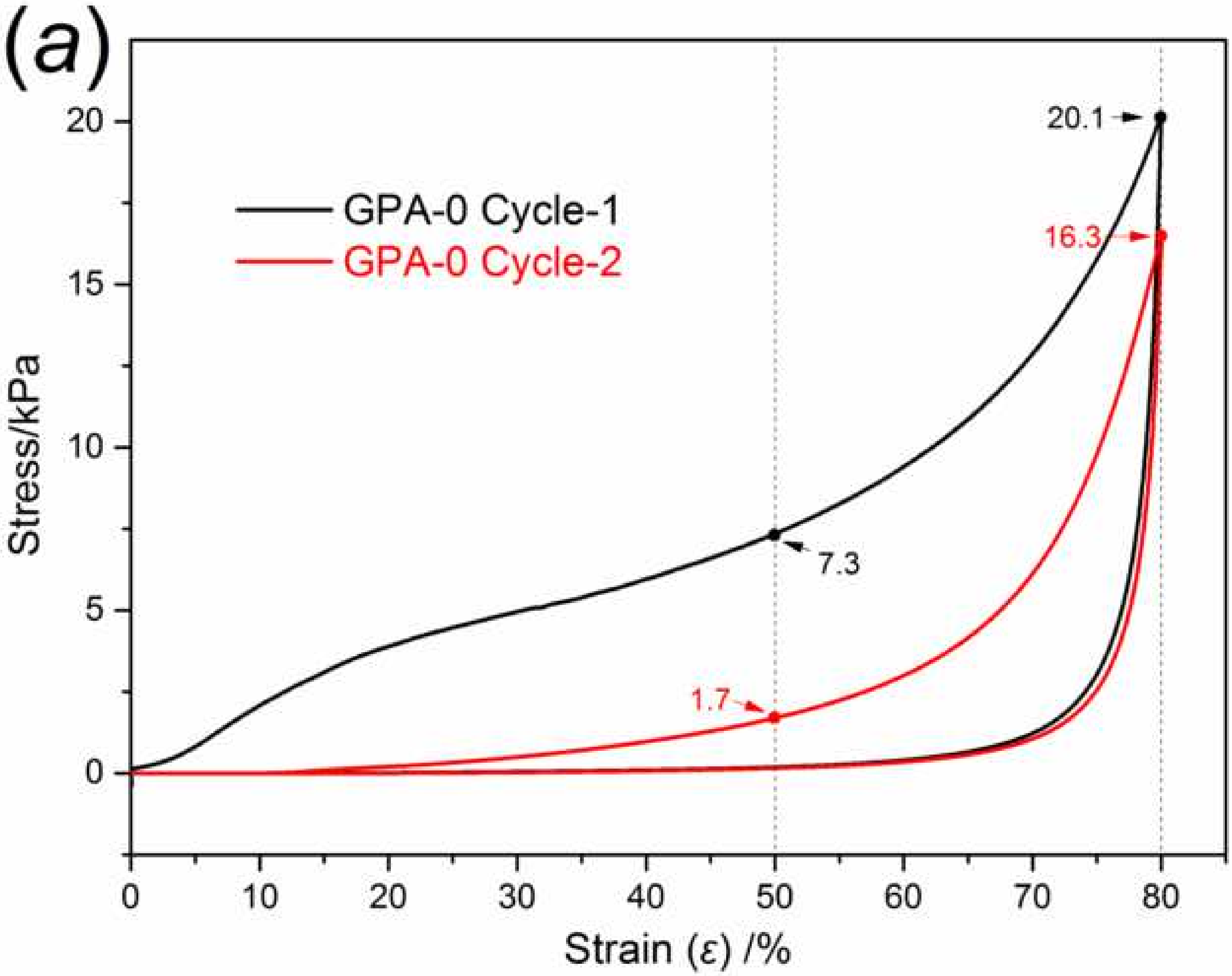
(a)
GPA-0 Cycle-1
GPA-0 Cycle-2
20.1
16.3
7.3
1.7
Stress/kPa
Strain (ε) /%
0
5
10
15
20
0
10
20
30
40
50
60
70
80

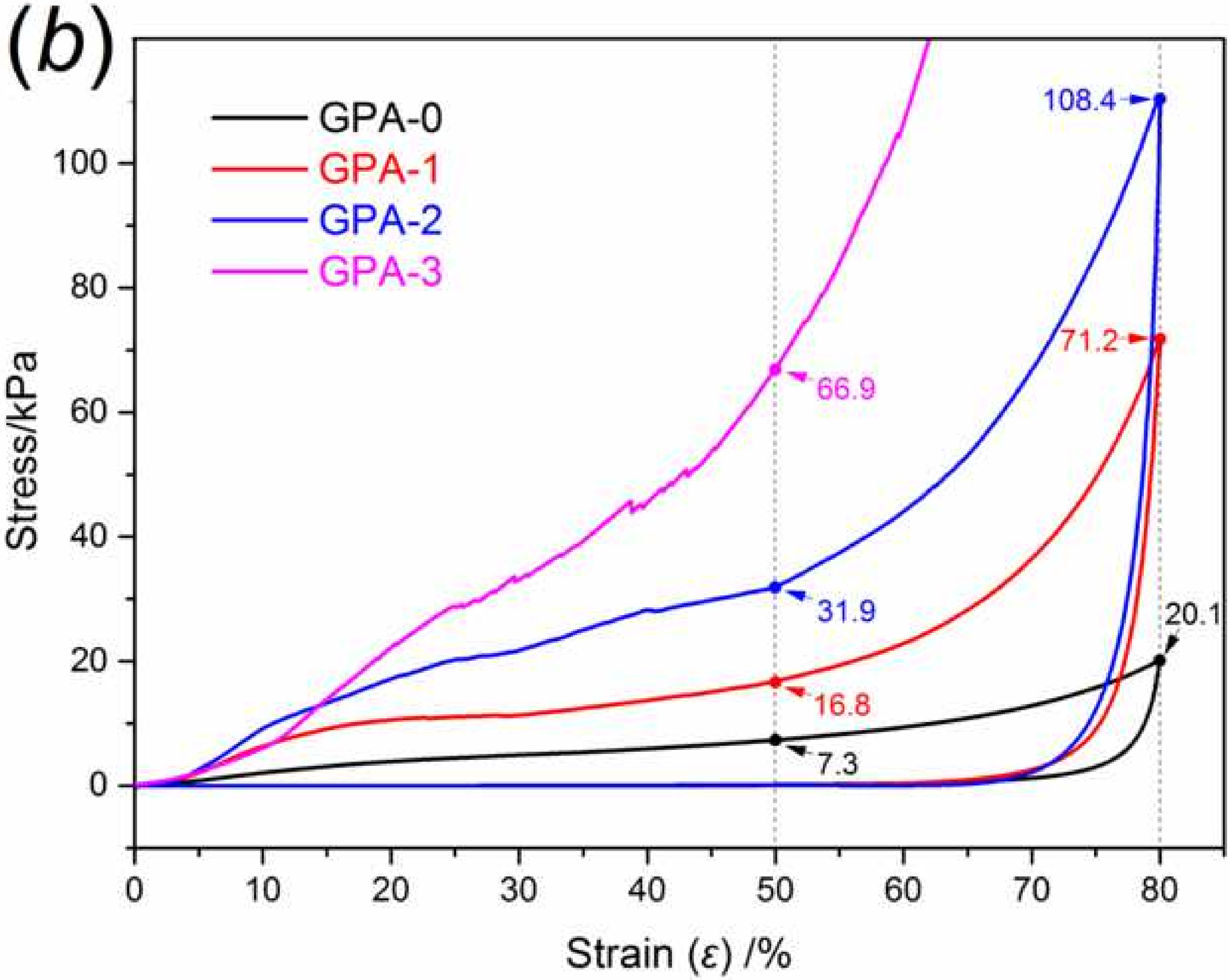
(b)
GPA-0
GPA-1
GPA-2
GPA-3
108.4
71.2
66.9
31.9
16.8
7.3
20.1
Stress/kPa
Strain (ε) /%
0
20
40
60
80
100
0
10
20
30
40
50
60
70
80

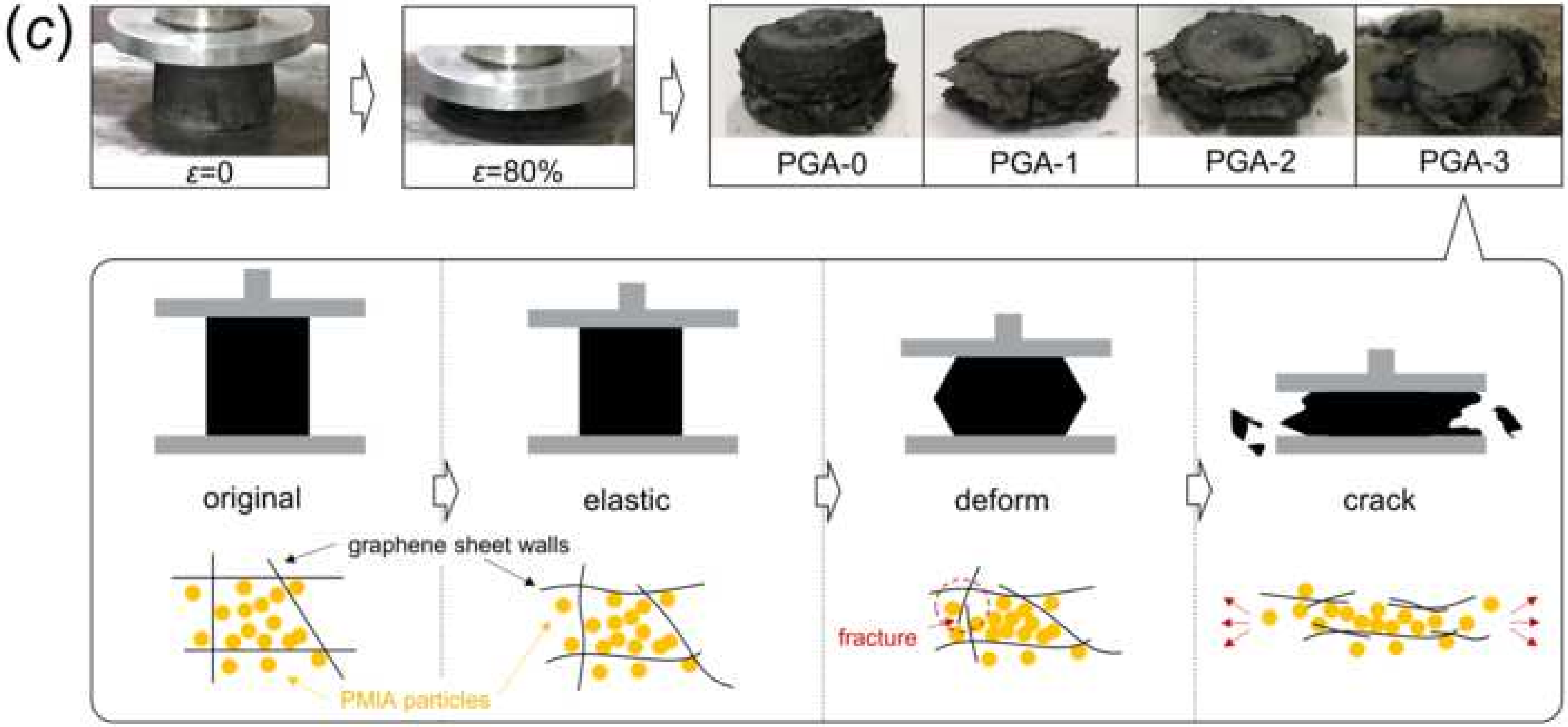
(c)
ε=0
ε=80%
PGA-0
PGA-1
PGA-2
PGA-3
original
elastic
deform
crack
graphene sheet walls
PMIA particles
fracture

Poly (*m*-phenylene isophthalamide)/Graphene Composite Aerogels with Enhanced Compressive Shape Stability for Thermal Insulation

Weiwang Chen, [1] Sha Liu, [1] Yutong Dong, [1] Xiaomeng Zhou, [1*] Fenglei Zhou, [2, 3]

[1] *Key Laboratory of Civil Aviation Thermal Hazards Prevention and Emergency Response, Civil Aviation University of China, Tianjin, 300300, P. R. China*

[2] *Centre for Medical Image Computing, Department of Computer Science, University College London, London, WC1V 6LJ, UK*

[3] *College of Textiles and Clothing, Qingdao University, Qingdao, 266071, P. R. China*

Address correspondence to E-mail: X. Zhou (E-mail: zhouxm@nankai.edu.cn)

Acknowledgements

This work was supported by National Natural Science Foundation of China (Grant No. 51904312), Shandong "Taishan Youth Scholar Program" and Research Start-up Funds of Civil Aviation University of China (600005140216). The authors are deeply grateful to these supports.

Table S1. The fabrication processes and properties of polymer-incorporated graphene aerogels.

NO.	GA composites	Polymers incorporated	Fabrication process	GA content wt. %	Density mg/cm^3	Rigid or Compressible	Normal press at 50% strain	Withstand high temperatures?	Thermal conductivity W/m K	Ref.
1	XPAA/rGO Aerogels.	Poly (acrylic anhydrides)	Premixed & Post thermal treatment	57-80	4.38-6.69	Compressible	<25 kPa	NO	—	1
2	GPA–PAA Aerogels.	Poly (acrylic acid)	Premixed	48-81	5.3-6.7	Compressible	~5 kPa	NO	—	2
3	GPA–PEO Aerogels.	Poly (ethylene oxide)	Premixed	72-81	4.2-4.6	Rigid	~3 kPa	NO	—	2
4	rGO/PI Aerogels.	Polyimide	Premixed & Post thermal treatment	—	~10	Compressible	~2.8 kPa	Yes	—	3
5	Silane bonded graphene aerogels	Silane coupling agents	Premixed	9-50	10-100	Compressible	6-14 kPa	No	—	4
6	GEAs	Epoxy	Premixed	3-9	90-93	Compressible	<10 kPa	No	—	5
7	CNS/CAs	Carbide of Resorcinol-formaldehyde	Premixed & Post Carbonization	5-50	23.5-70.5	Rigid	Crack at 10-20% strain	Yes	0.027-0.035	6
8	CMC/GO/BA	Carboxymethyl Cellulose with boric acid as cross-linker	Premixed	0.1-5	25	Compressible	~80 kPa	No	0.042-0.046	7
9	GAPC	Polydimethylsiloxane	post-impregnated	0.2-1	—	Compressible	1-10 MPa	Yes	0.5-0.58	8
10	GO-WPU	Waterborne polyurethane	post-impregnated	—	16-27	Compressible	~20 kPa	No	~0.025	9
11	PVA/CNF/GONS	polyvinyl alcohol with and without cellulose nanofibrils	Premixed	—	18-35	—	<20kPa	No	0.045	10
12	PGAs	poly (*m*-phenylene isophthalamide)	Premixed	~3-26	19.3-76	Rigid	16.8-66.9 kPa	Yes	0.036-0.044	This work

References

1. Ha, H.; Shanmuganathan, K.; Ellison, C. J., Mechanically stable thermally crosslinked poly(acrylic acid)/reduced graphene oxide aerogels. *ACS Appl Mater Inter* **2015,** *7*, 6220-6229.

2. Lu, H.; Li, C.; Zhang, B.; Qiao, X.; Liu, C., Toward highly compressible graphene aerogels of enhanced mechanical performance with polymer. *RSC Adv* **2016,** *6*, 43007-43015.
3. Qin, Y.; Peng, Q.; Ding, Y.; Lin, Z.; Wang, C.; Li, Y.; Xu, F.; Li, J.; Yuan, Y.; He, X.; Li, Y., Lightweight, superelastic, and mechanically flexible graphene/polyimide nanocomposite foam for strain sensor application. *ACS Nano* **2015,** *9*, 8933-8941.
4. Guan, L.; Gao, J.; Pei, Y.; et al., Silane bonded graphene aerogels with tunable functionality and reversible compressibility. *Carbon* **2016,** *107*, 573-582.
5. Ye, S.; Feng, J.; Wu, P., Highly elastic graphene oxide–epoxy composite aerogels via simple freeze-drying and subsequent routine curing. *J Mater Chem A* **2013,** *1*, 3495-3502.
6. Sun, W.; Du, A.; Gao, G.; et al., Graphene-templated carbon aerogels combining with ultra-high electrical conductivity and ultra-low thermal conductivity. *Micropor Mesopor Mater* **2017,** *253*, 71-79.
7. Ge, X.; Shan, Y.; Wu, L.; et al., High-strength and morphology-controlled aerogel based on carboxymethyl cellulose and graphene oxide. *Carbohyd Polym* **2018,** 277-283.
8. Zhang, Q.; Xu, X.; Li, H.; et al., Mechanically robust honeycomb graphene aerogel multifunctional polymer composites. *Carbon* **2015,** *93*, 659-670.
9. Sun, F.; Yang, J.; Zhang, H.; et al., Multi-functional composite aerogels enabled by chemical integration of graphene oxide and waterborne polyurethane via a facile and green method. *Composi Sci Technol* **2018,** 175-182.
10. Javadi, A.; Zheng, Q.; Payen, F.; et al., Polyvinyl alcohol-cellulose nanofibrils-graphene oxide hybrid organic aerogels. *ACS Appl Mater Inter* **2013,** *5,* 5969-5975.